NASA
Technical
Paper
1928

December 1981

Aerodynamic Heating on the Corrugated Surface of a 10.2° Half-Angle Blunted Cone at Mach 6.7

Irving Weinstein,
Don E. Avery,
and L. Roane Hunt

NASA

NASA Technical Paper 1928

1981

Aerodynamic Heating on the Corrugated Surface of a 10.2° Half-Angle Blunted Cone at Mach 6.7

Irving Weinstein,
Don E. Avery,
and L. Roane Hunt
Langley Research Center
Hampton, Virginia

NASA
National Aeronautics
and Space Administration

Scientific and Technical Information Branch

SUMMARY

An experimental investigation was conducted to determine the aerodynamic heating over the corrugated surface of a 10.2° half-angle blunted cone. The model had a 15.2 cm nose radius and 36 insulated corrugated panels distributed over the surface of the cone. The tests were conducted in the Langley 8-Foot High-Temperature Structures Tunnel in a test medium of methane-air combustion products at a nominal Mach number of 6.7 and a nominal total temperature of 1850 K. The tests were made at free-stream dynamic pressures of about 25 and 62 kPa, at free-stream Reynolds numbers from 1.8×10^6 to 4.8×10^6 per meter, and at angles of attack of 0°, 5°, and 10°.

The results show that the pressures measured on the windward side of the cone were generally underpredicted by smooth-cone theory. The pressures on the lee side of the model were also high and not in agreement with theory, apparently due to the influence of a high base pressure resulting from flow-blockage effects. At angles of attack there was an apparent minimal gas flow through the panel joints on the windward side of the model, probably allowing the flow to vent internally through the model support sting but causing no internal damage.

The aerodynamic heating measured over the corrugated surface on the windward side of the cone was in reasonable agreement with the theoretical turbulent prediction for a smooth cone. The heating measured on the leeward side was about halfway between laminar and turbulent predictions resulting from local transitional flow or flow separation produced by the high lee side pressures. The heating on the corrugation crests on the windward side was approximately 10 percent higher than that measured along the flats. This was expected since the boundary layer was thinner at the corrugation crest than in the flat region between corrugations. Localized heating measurements indicated a significant increase in heating for a cross-flow angle of 14.3°, with the maximum heating rates occurring on the upstream side of the corrugation crest and the minimum occurring on the downstream side. This effect of local flow separation and reattachment is similar to that obtained for corrugated flat panels.

INTRODUCTION

Future space transportation vehicles will be reusable and in order to keep the operating costs low these vehicles should require a minimum amount of repair or refurbishment. (See refs. 1 and 2.) Due to the extreme environments to which these transport systems are exposed, a thermal protection system (TPS) is required. One type of thermal protection system which has the capability of meeting these requirements consists of metallic corrugated panels placed over the surface to protect the primary structure. The corrugations, aligned in the flow direction, provide longitudinal stiffness to the surface. During normal flight and turning maneuvers, the corrugations may be yawed to the local flow which could have an effect on the aerodynamic heating which in turn affects the evaluation and design of the thermal protection system. Several corrugated flat-panel systems have been tested and evaluated in references 3 to 8, with the tests in reference 8 being done over a range of yaw angles.

The present investigation was conducted using a large 10.2° half-angle spherically blunted cone. Local aerodynamic heating-rate distributions were measured over realistic three-dimensional corrugated curved surfaces and a comparison was made of the results with theoretical predictions for a smooth surface. The test surface consisted of 36 corrugated panels distributed over the surface of a cone having a nose radius of 15.2 cm. The panels were insulated and attached to the primary structure with flexible stand-off clips which allowed for thermal expansion. The panel design is typical of the TPS concept described in reference 9. The tests were conducted in the Langley 8-Foot High-Temperature Structures Tunnel at a nominal Mach number of 6.7 and at a total temperature of about 1850 K. The tests were conducted at free-stream dynamic pressures of about 25 and 62 kPa, at free-stream Reynolds numbers from 1.8×10^6 to 4.8×10^6 per meter, and at angles of attack of 0°, 5°, and 10°.

Use of trade names in this report does not constitute an official endorsement of such products or manufacturers, either expressed or implied, by the National Aeronautics and Space Administration.

SYMBOLS

c	specific heat of material, J/kg-K
d	pitch of panel corrugation (fig. 5), cm
ℓ	circumferential distance measured from panel centerline (fig. 5), cm
M	Mach number
p	pressure, Pa
q	dynamic pressure, Pa
$\dot{q}$	heating rate, W/m^2
R	unit Reynolds number, m^{-1}
r	model nose radius (fig. 4), cm
s	surface distance measured from nose on body axis (fig. 4), cm
T	temperature, K
t	time, sec
α	angle of attack (fig. 4), deg
β	meridian angle (fig. 4), deg
γ	ratio of specific heats
δ	boundary-layer thickness, cm
ϵ	maximum wave amplitude of corrugations (fig. 3), cm

θ cross-flow angle, deg

ρ material density, kg/m^3

τ material thickness, cm

ϕ local corrugation angle (fig. 5), deg

Subscripts:

t total conditions

s stagnation point

∞ free-stream conditions

APPARATUS AND TESTS

Model

The model was a 10.2° half-angle spherically blunted cone which had a nose radius of 15.2 cm. A smooth surface version of this model was tested first to obtain tunnel blockage information and some preliminary surface pressure data. The corrugated-surface version of this model is shown schematically in figure 1. The nose was constructed of a tantalum 10-percent tungsten material 1.5 mm thick and coated for protection at high temperatures. The surface of the cone frustrum consisted of an array of 36 corrugated panels. The model had an overall length of 203.3 cm and a base diameter of 91.4 cm. A photograph of the test model is shown in figure 2 mounted on the sting and curved strut support system in the Langley 8-Foot High-Temperature Structures Tunnel. The painted grid on the side of the model was used as a reference for photographs.

Details of a typical curved metallic panel are shown in figure 3. The panel surface is corrugation stiffened in the longitudinal direction. The corrugations are circular-arc segments connected by straight-line segments as shown in figure 3. The pitch of the corrugations is 3.81 cm and the flats between corrugations are 0.64 cm wide. The amplitude of the corrugations is 0.48 cm. This geometry is the same as that used in reference 9. Two hat-shaped support sections were spot-welded to the flats of each panel transverse to the corrugations. Two C-shaped stand-off clips, which allowed for expansion and contraction, were spot-welded to each hat section. Holes through the panel, hat section, and clip provided access for attachment and removal of the panels from the primary structure. Snap-on metallic plugs were used to close these access holes and minimize the ingress of hot gases into the model. The crests of the corrugations of the forward row of panels fair into the nose section such that there are rearward facing steps in the vicinity of the panel flats as indicated in the section view of figure 1. The panel side edges were stiffened and overlapped as shown in figure 3 to close out the edges and provide a sliding expansion joint. The rear edge of each panel overlaps the next downstream panel to allow for longitudinal thermal growth and to minimize the ingress of hot gases.

An identification scheme for the panels is shown in the schematic in figure 4. There were four circumferential rows with nine panels in each row. The leading edge of the first row of panels started behind the nose at an s/r of 3.52. The four circumferential rows were identified as 1 through 4 starting with the upstream row

and the nine panels in each row were designated A through I in a counterclockwise direction with the centerline of A being on the windward meridian. Different materials were used for the various panels according to their capability to withstand the expected temperatures at various locations. The panel materials are indicated on the inset of figure 4. Nine of the panels were made of Haynes alloy No. 25 (trademark of Cabot Corp.) which has a cobalt base, 6 were made of Inconel 718 (trademark of The International Nickel Co., Inc.), 20 were made of René 41 (trademark of Allvac Metals Co.) which has a nickel base, and 1 was made of TD Nickel-Chrome. The Haynes 25 panels, which were on the windward side of the model, had a nominal thickness of 0.64 mm and all other panels had a nominal thickness of 0.25 mm.

The centerline of each longitudinal row of panels coincides with a model meridian line. However, the corrugations are parallel to each other and a surface angle ϕ is formed between the corrugation line and the meridian lines for all locations off the panel centerline. Figure 5 shows a plot of ϕ as a function of s/r and ℓ/d. The value of ϕ approaches 4° near the edge of each panel.

A low density insulation was used between the panels and the base structure to minimize the heat transfer to the primary structure. The insulation was cut to cover the back surface of the panel. It was then slotted to fit around the standoff clips and against the backside of the panel. One 0.6-cm-thick sheet of felt insulation (Dynaflex: trademark of Johns-Manville Corporation) was placed onto the panel first and then two layers of a fibrous silica insulation (Micro-Quartz: trademark of Johns-Manville Corporation) were added to form an insulation package lightly compressed to approximately 0.5 cm. The top and bottom views of a corrugated panel with insulation attached are shown in figure 6.

Instrumentation

Nine pressure orifices were located on the outer surface of the smooth-surface cone, as indicated in table I. On the corrugated cone, temperatures were measured at 131 locations on the test panels as indicated in figure 7 using No. 30 chromel-alumel thermocouple wire. Surface pressures and pressures on the backside of the panel were measured at the three locations shown in figure 7. The figure shows a projected front view of the model with the instrumentation attached behind the panels at the locations indicated. The dashed lines represent the center of the flats between corrugations. Sections A-A and B-B were heavily instrumented with thermocouples across a corrugation as indicated on the enlarged view of sections A-A and B-B on figure 7. Tables I and II identify the general pressure-orifice and thermocouple locations on each panel and the specific locations in terms of the surface distance s/r, the circumferential angle β measured from the windward vertical plane meridian, and the surface distance off the panel centerline ℓ/d.

Figure 8 shows a typical thermocouple and pressure-orifice installation on the back of a panel. The thermocouples were each enclosed in a stainless steel tube for protection from high temperatures and the ends of the wires were fed through a two-hole ceramic bead to keep the wires separated. The wires were aligned in the flow direction and spot-welded to the panel side by side at the same longitudinal location. The end of the sheathing was strapped down with stainless steel strips spot-welded to the panel. The surface pressure orifice extended through the panel on a flat between corrugations and was ground flush with the outer surface. An orifice support plate was welded to a flat on the backside of the panel. The orifice used to

measure the backside pressure was placed as shown in figure 8 and both pressure tubes were strapped together with stainless-steel strips placed over the tubing and spot-welded to the panel.

Facility

The tests were conducted in the Langley 8-Foot High-Temperature Structures Tunnel which is shown schematically in figure 9. This facility is a hypersonic blowdown wind tunnel which develops high energy by burning a mixture of methane and air under pressure in a combustion chamber. The combustion products are then expanded through an axisymmetric conical contoured nozzle having an exit diameter of 2.4 m and then into the test section where the products of combustion serve as the test medium. The test section has a usable test core approximately 1.2 m in diameter. The flow then goes through a supersonic diffuser and is pumped to the atmosphere by means of a single-stage annular air ejector. The tunnel operates at a nominal Mach number of 7, at free-stream dynamic pressures from 14 to 86 kPa, and at total temperatures from 1390 to 2000 K. These conditions correspond to free-stream unit Reynolds numbers between 1×10^6 and 10×10^6 per meter and simulate altitudes between 25 and 40 km. A model pitch system provides an angle-of-attack range of $\pm 20°$. Additional details of this test facility may be found in references 10 and 11.

Test Procedure

The tests were conducted by starting the tunnel while the model was held in a pod below the test section. The model was protected from tunnel start-up and shut-down loads with acoustic covers. After steady tunnel flow was established, the acoustic covers were retracted and the model was inserted rapidly into the test stream as the model was pitched to the desired angle of attack. This rapid insertion (approx 1.5 sec) gave the model an effective step-function exposure to the stream, thus allowing cold-wall heating rates to be determined. Prior to tunnel shutdown, the model was withdrawn from the stream and covered with the acoustic covers.

Table III shows the test conditions for the smooth-cone model and the 10 runs for the 10.2° blunted-cone model. The tests were made at tunnel total temperatures from 1750 K to 1980 K and at both a high and a low range of free-stream Reynolds numbers as indicated in table III. The free-stream test conditions were determined from temperatures and pressures measured in the combustor using the thermal, transport, and flow properties of methane-air combustion products reported in reference 12 and the tunnel surveys of reference 10. The model stagnation-point pressures were obtained from tunnel survey charts and the stagnation-point heating rates were obtained by the method of reference 13.

Data Reduction

Model and tunnel thermocouple and pressure-transducer outputs were recorded at the Langley Central Digital Data Recording Facility at 20 samples per second and were converted to temperatures and pressures. The model temperature data were smoothed by fitting a third-order polynomial to the first 20 points of data starting 1 sec before the model reaches the tunnel centerline. Successive curve segments were obtained by shifting 10 time increments, curve fitting 20 data points, retaining the first half of the curve fit each time, and then fairing the curve segments. The panel surface heating rates were then obtained by using the slope of the composite curve at the

time the model reached the tunnel centerline in the one-dimensional heat-balance equation, $q = \rho c \tau \, dT/dt$. The effects of radiation and lateral conduction were neglected since the temperature-time slopes were taken early in the tests when the surface temperatures and temperature gradients were relatively low.

FLOW ANALYSIS

The flow over the model was analyzed assuming a perfect-gas solution for air at $\gamma = 1.4$ and a Mach number of 6.8. The free-stream static pressure and temperature used for the analysis were 2.0 kPa and 230 K, respectively. The model stagnation pressure and heating rate used were 120 kPa and 0.63 MW/m^2, respectively. The theoretical values for pressure along the cone were calculated by obtaining the inviscid-flow solution for a smooth blunt cone using the finite-difference marching technique described in references 14 and 15. The laminar heating over the cone surface was then calculated using the surface pressures from the inviscid-flow solution and the boundary-layer solution in reference 16. The boundary-layer solution uses an axisymmetric analogue to reduce the three-dimensional boundary-layer equations along surface streamlines to an equivalent axisymmetric form. The turbulent heating was calculated using pressure data from the inviscid-flow solution along with the turbulent boundary-layer computer code developed in reference 17. The experimental data were obtained in combustion products while the properties for air were used in the theoretical programs. Reference 18 shows good correlation of data obtained in air with that for combustion products when normalized to the stagnation-point values; therefore, the comparisons of experimental and theoretical normalized results are considered valid. It should also be pointed out that all calculations were made for a smooth wall without corrugations.

RESULTS AND DISCUSSION

Pressure Distributions

The pressure distributions along the windward vertical-plane meridian for angles of attack of 0°, 5°, and 9.9° are presented in figure 10, with the pressures being normalized to the stagnation-point pressure. The solid curves represent the theoretical distributions at $\beta = 0°$ obtained from the inviscid-flow solution described in references 14 and 15 for a 10.2° blunted smooth cone. The dashed lines represent the equivalent sharp-cone pressure levels obtained from reference 19. The trend of the pressure distribution obtained from the smooth cone for $\alpha = 0°$ agrees with the theory and the magnitude is about 10 percent above the theory. Measured pressures from the tests for the corrugated cone were obtained only at the one longitudinal location of $s/r = 10.6$ with the nearest windward measurements made at $\beta = 5.6°$. The corrugated-cone data is about 20 percent above theory at $\alpha = 0°$ and departs more from the theory at higher angles of attack.

The circumferential pressure distributions at $s/r = 10.6$ for the three angles of attack are shown in figure 11. The pressures on the surface of the panels are indicated with the open symbols and the pressures under the panels are shown with solid symbols. The theoretical values are presented as solid curves. As indicated in figure 10, the surface pressures near the windward meridian were underpredicted by theory. However, the trend of the data with meridian angle β shows general agreement with theory near the side and on the windward portion of the model. At these locations both the surface and backside pressures increased with α, but an inward pressure difference was maintained indicating inward gas flow. The flow through the

panel joints probably vented through the sting to a low pressure region in the pod below the test section. This flow was evidently minimal as there was no apparent internal damage to the insulation that was packed against the inner surface of each panel. The pressure was in agreement with theory on the leeward surface ($\beta = 154.4°$) for $\alpha = 0°$ and was not affected by the high model base pressure indicated in figure 11. However, the leeward surface pressure was much higher than theory as the angle of attack was increased. The pressure in this region was apparently influenced by the high base pressure caused by tunnel flow blockage of the large model. The high pressure in the base must have fed forward and disturbed the normal lee-side flow pattern.

Heating Distributions

Longitudinal.- Typical longitudinal heating-rate distributions along the windward meridian for tests 3, 4, and 5 at nominal angles of attack of 0°, 5°, and 10°, respectively, are shown in figure 12. The local heating is normalized to the stagnation-point heating rate. The data were obtained on the panel centerline flat between corrugations, and the thermocouples in the vicinity of panel overlap are not included as the heating would understandably be very low since the surface there is shielded from exposure to the flow. The heating for $\alpha = 0°$ decreases gradually with increasing longitudinal distance while the heating increases with distance for angles of attack of 5° and 9.9°. At any given longitudinal location, the heating increases with an increase in angle of attack with the greatest differences occurring at the rear of the model.

The normalized longitudinal heating distributions are shown in figure 13 along the panel centerline flat and on the crest of the adjacent corrugation for $\alpha = 0°$, 5°, and 9.9°. The panel centerline flat was along the windward vertical-plane meridian and the thermocouples on the adjacent crest ranged from 2.5° to 5.4° off the windward meridian. The data obtained from the corrugation crest are indicated with the flagged symbols. The laminar- and turbulent-heating theories from references 16 and 17, respectively, are also shown in figure 13. A comparison of the data with theory indicates that the flow on the cone was turbulent on the windward surface for all angles of attack tested although the turbulent theory generally overpredicted the measured data. Theoretical predictions of measured heating rates with a turbulent boundary layer are generally high for this facility. (See, for example, the smooth flat plate results of ref. 10.) Therefore, these measured heating rates were about equal to that expected for a smooth surface, with any discrete effects of the corrugations being washed out by flow disturbances due to panel overlap and other surface discontinuities. This also indicates that there was no additional surface heating penalty associated with the corrugated surface for these tests. Some of the increase in heating to the rear of the model at the higher angles of attack is predicted by theory although some of this increase may be due to a bleeding of the boundary-layer gases around the panels on the windward meridian as described earlier. The heating measured on the corrugation crests is about 10 percent higher than the heating measured on the flats near the windward meridian for all angles of attack tested. This would be expected since the boundary layer would be thinner at the corrugation crest than in the region of the flat between corrugations. A similar heating trend is shown in reference 8 over a corrugated surface.

Circumferential.- The heating rates obtained on the flat at the center of the panels are presented as circumferential distributions in figure 14 for three longitudinal locations. These locations correspond to the midlength of each of the first three circumferential rows of panels as indicated in figure 4. The heating is

approximately constant at $\alpha = 0°$ for all three s/r locations except for a drop in the heating along the side of the model. The heating distributions for $\alpha = 5°$ and $9.9°$ are reasonably flat from the windward meridian around the body to $\pm 40°$ for s/r values of 5.03 and 7.8 and then reduce rapidly around the leeward side. For $s/r = 10.6$, the heating reduces rapidly from the windward meridian around to the leeward side. Generally, the heating on the leeward side is lowest for the highest angle of attack at all s/r locations.

The measured circumferential heating distributions are shown in figure 15 for an s/r value of 7.8 and include the heating on the crests of the corrugations as well as on the flats between corrugations. The heating distributions given by the laminar and turbulent theories are also shown. The flagged points again represent the heating on the crests which seem to be slightly higher than on the flats near the windward meridian but slightly lower near the leeward side. The heating generally agrees with turbulent theory from the windward side to about $\beta = \pm 50°$ for all angles tested. With a further increase in β toward the leeward side the heating falls considerably below turbulent theory to a value about halfway between the turbulent and laminar theories. This characteristic may be a result of transitional flow on this portion of the model or it could have been caused by flow separation produced by the high lee-side pressures. Attached flow was assumed for the theory and neither transition nor separated flow were considered.

Local heating.- As the angle of attack is increased on a configuration which has corrugated surfaces, a cross flow over the corrugations occurs which could have an effect on the heating over the surfaces. To check these cross-flow effects, typical heating distributions, which were obtained across heavily instrumented corrugations, are presented in figures 16 and 17 for the low and high Reynolds number range, respectively. The instrumented corrugations are located at meridian angles β of approximately 30° and 70° at a longitudinal location of $s/r = 7.8$ which corresponds to the midlength of the second circumferential row of panels. The cross-flow angle θ between the local streamline and the corrugation was the sum of the flow angularity computed using reference 16 and the corrugation correction angle ϕ defined by the curves in figure 5. At a β value of approximately 30° (fig. 16) the heating is relatively constant across the corrugation for both Reynolds numbers at all angles of attack tested. For $\beta = 70°$ (fig. 17), the heating is approximately constant for $\alpha = 0°$. As α increases to 10° where the cross-flow angle θ is 14.3°, the maximum heating rates occur on the windward side of the corrugation crests and the minimum values occur on the leeward side. Evidently, the flow separates on the downstream side producing reduced heating and reattaches on the upstream side of the next corrugation producing increased heating. These distributions are similar to those obtained in reference 8 on a two-dimensional corrugated surface for cross-flow angles above 15°. The ratio of the maximum heating on the windward side of the corrugation to the minimum measured on the leeward side for a cross-flow angle of 14.3° is between 3 and 4 for the present tests while the ratio is 2 at a cross-flow angle of 15° for the data of reference 8. This is as expected since the ratio of the boundary-layer thickness to the corrugation amplitude δ/ε is much smaller (thinner boundary layer) for the present data. Even greater peak heating could be expected for local-flow reattachment at higher cross-flow angles as indicated in reference 8.

CONCLUDING REMARKS

An experimental investigation was conducted in the Langley 8-Foot High-Temperature Structures Tunnel to determine the aerodynamic heating over the corrugated surfaces of a 10.2° half-angle blunted cone. The model had a 15.2 cm nose radius and had 36 insulated corrugated panels distributed over the surface of the cone. The tests were conducted in a test medium of methane-air combustion products at a nominal Mach number of 6.7 and a nominal total temperature of 1850 K. The tests were made at free-stream dynamic pressures of about 25 and 62 kPa, at free-stream Reynolds numbers from 1.8×10^6 to 4.8×10^6 per meter, and at nominal angles of attack of 0°, 5°, and 10°.

The results show that the pressures measured on the windward side of the cone were generally underpredicted by smooth-cone theory; however, the trend in the circumferential direction agreed with the theory. The pressures on the lee side of the model were high and not in agreement with theory, apparently due to the influence of a high base pressure resulting from flow-blockage effects. For the angle-of-attack cases, there was an apparent minimal gas flow through the panel joints on the windward side of the model allowing the flow to vent internally through the model support sting but causing no internal damage.

The aerodynamic heating measured over the corrugated surface on the windward side of the cone was in reasonable agreement with the theoretical turbulent prediction for a smooth cone, and any discrete effects of the corrugations are probably washed out by flow disturbances due to panel overlap and other surface discontinuities. The heating measured on the leeward side was about halfway between laminar and turbulent predictions resulting from local transitional flow or flow separation produced by the high lee-side pressures. The heating on the corrugation crests on the windward side was approximately 10 percent higher than that measured along the flats which was as expected since the boundary layer would be thinner at the corrugation crest than in the region of the flat between corrugations. Localized heating measurements indicated a significant increase in heating for a cross-flow angle of 14.3°, with the maximum heating rates occurring on the upstream side of the corrugation crest and the minimum occurring on the downstream side. This effect of local flow separation and reattachment is similar to that obtained for corrugated flat panels.

Langley Research Center
National Aeronautics and Space Administration
Hampton, VA 23665
September 30, 1981

REFERENCES

1. Anderson, Roger A.; Brooks, William A., Jr.; Leonard, Robert W.; and Maltz, Joseph: Structures - A Technology Overview. Astronaut. & Aeronaut., vol. 9, no. 2, Feb. 1971, pp. 38-47.

2. Kelly, H. Neale; Rummler, Donald R.; and Jackson, L. Robert: Research in Structures and Materials for Future Space Transportation Systems - An Overview. A Collection of Technical Papers - AIAA/NASA Conference on Advanced Technology for Future Space Systems, May 1979, pp. 12-23. (Available as AIAA Paper 79-0859.)

3. Deveikis, William D.; Miserentino, Robert; Weinstein, Irving; and Shideler, John L.: Aerothermal Performance and Structural Integrity of a René 41 Thermal Protection System at Mach 6.6. NASA TN D-7943, 1975.

4. Sawyer, James Wayne: Aerothermal and Structural Performance of a Cobalt-Base Superalloy Thermal Protection System at Mach 6.6. NASA TN D-8415, 1977.

5. Avery, Don E.: Performance of a Haynes 188® Metallic Standoff Thermal Protection System at Mach 7. NASA TP-1802, 1981.

6. Brandon, Harold J.; Britt, Allen H.; and Dunavant, James C.: Aerothermodynamic Assessment of Corrugated Panel Thermal Protection Systems. AIAA Paper 78-841, May 1978.

7. Bohon, Herman L.; Shideler, John L.; and Rummler, Donald R.: Radiative Metallic Thermal Protection System: A Status Report. J. Spacecr. & Rockets, vol. 14, no. 10, Oct. 1977, pp. 626-631.

8. Sawyer, James Wayne: Pressure and Heating-Rate Distributions on a Corrugated Surface in a Supersonic Turbulent Boundary Layer. NASA TP-1024, 1977.

9. Wichorek, Gregory R.; and Stein, Bland A.: Experimental Investigation of Aluminide-Coated Ta-10W for Heat-Shield Applications. NASA TN D-5524, 1969.

10. Deveikis, William D.; and Hunt, L. Roane: Loading and Heating of a Large Flat Plate at Mach 7 in the Langley 8-Foot High-Temperature Structures Tunnel. NASA TN D-7275, 1973.

11. Deveikis, William D.; Bruce, Walter E., Jr.; and Karns, John R.: Techniques for Aerothermal Tests of Large, Flightweight Thermal Protection Panels in a Mach 7 Wind Tunnel. NASA TM X-71983, 1974.

12. Leyhe, Edward W.; and Howell, Robert R.: Calculation Procedure for Thermodynamic, Transport, and Flow Properties of the Combustion Products of a Hydrocarbon Fuel Mixture Burned in Air With Results for Ethylene-Air and Methane-Air Mixtures. NASA TN D-914, 1962.

13. Fay, J. A.; and Riddell, F. R.: Theory of Stagnation Point Heat Transfer in Dissociated Air. J. Aeronaut. Sci., vol. 25, no. 2, Feb. 1958, pp. 73-85, 121.

14. Marconi, Frank; Salas, Manuel; and Yaeger, Larry: Development of a Computer Code for Calculating the Steady Super/Hypersonic Inviscid Flow Around Real Configurations. Volume I - Computational Technique. NASA CR-2675, 1976.

15. Marconi, Frank; and Yaeger, Larry: Development of a Computer Code for Calculating the Steady Super/Hypersonic Inviscid Flow Around Real Configurations. Volume II - Code Description. NASA CR-2676, 1976.

16. Hamilton, H. Harris, II: Calculation of Laminar Heating Rates on Three-Dimensional Configurations Using the Axisymmetric Analogue. NASA TP-1698, 1980.

17. Miner, E. W.; Anderson, E. C.; and Lewis, Clark H.: A Computer Program for Two-Dimensional and Axisymmetric Nonreacting Perfect Gas and Equilibrium Chemically Reacting Laminar, Transitional and/or Turbulent Boundary Layer Flows. VPI-E-71-8, May 1971. (Available as NASA CR-132601.)

18. Weinstein, Irving: Heat-Transfer and Pressure Distributions on Hemisphere-Cylinders in Methane-Air Combustion Products at Mach 7. NASA TN D-7104, 1973.

19. Ames Research Staff: Equations, Tables, and Charts for Compressible Flow. NACA Rep. 1135, 1953. (Supersedes NACA TN 1428.)

TABLE I.- PRESSURE ORIFICE LOCATIONS ON MODELS

Orifice no.	Panel no.	s/r	ℓ/d	β, deg
Corrugated model				
1	3A	10.60	1.00	5.6
2	3A	↓	1.00	5.6
3	3C		-1.00	74.4
4	3C		-1.00	74.4
5	3E		-1.00	154.4
6	3E		-1.00	154.4
Smooth cone model				
1		2.38		33
2		2.84		33
3		3.31		-45
4		5.22		33
5		6.83		33
6		8.97		33
7		10.96		33
8		11.43		33
9		11.90		60

TABLE II.- THERMOCOUPLE LOCATIONS ON PANELS

Thermocouple no.	Panel no.	Location on panel (a)	s/r	ℓ/d	β,deg
1	1A	E	3.60	1.67	18.9
2		F		0	0
3		C		-.50	-5.4
4		F		-1.00	-10.7
5		E		-1.68	-18.9
6		F	4.06	0	0
7		S	4.26	0	0
8		S		-1.00	-9.9
9		S		-1.50	-14.8
10		E	5.03	2.00	18.1
11		F		0	0
12		C		-.50	-4.5
13		F		-1.00	-9.0
14		C		-1.50	-13.6
15		F		-2.00	-18.1
16		E		-2.23	-19.3
17		F	5.56	0	0
18		S	5.75	0	0
19		S	5.75	-1.92	-16.7
20		E	6.37	2.33	19.0
21		F		0	0
22		C		-.50	-4.0
23		E		-2.37	-19.0
24	2A	E	6.50	2.33	18.6
25		F		0	0
26		E		-2.33	-18.6
27		F	6.92	0	0
28		S	7.08	0	0
29		E	7.80	2.62	18.9
30		F		0	0
31		C		-.50	-3.4
32		C		-1.50	-10.3
33		E		-2.62	-18.9
34		S	8.52	0	0
35		E	9.07	2.95	18.8
36		F		0	0
37		E		-2.95	-18.8
38	3A	F	9.20	0	0
39		F	10.60	0	0
40		C		-.50	-2.8
41		C		-1.50	-8.4

[a]C - Corrugation
E - Edge
F - Flat
S - Support

TABLE II.- Continued

Thermocouple no.	Panel no.	Location on panel (a)	s/r	ℓ/d	β, deg
42	3A	C	10.60	-2.50	-14.0
43	3A	F	11.78	0	0
44	4A	F	12.31	0	0
45	↓	C	↓	-.50	-2.5
46	↓	C	↓	-1.50	-7.5
47	↓	C	↓	-2.50	-12.5
48	1B	F	3.60	0	40.0
49	↓	E	5.03	2.13	58.1
50	↓	C	↓	1.50	53.6
51	↓	F	↓	0	40.0
52	↓	C	↓	-1.50	26.5
53	↓	E	↓	-2.07	20.7
54	↓	F	6.37	0	40.0
55	2B	F	6.50	0	40.0
56	↓	E	7.80	2.85	58.9
57	↓	C	↓	1.50	50.3
58	↓	F	↓	0	40.0
59	↓	C	↓	-.50	36.6
60	↓	F	↓	-.972	33.3
61	↓	F	↓	-1.028	32.9
62	↓	C	↓	-1.178	31.8
63	↓	C	↓	-1.285	31.1
64	↓	C	↓	-1.392	30.4
65	↓	C	↓	-1.50	29.7
66	↓	C	↓	-1.608	29.0
67	↓	C	↓	-1.715	28.3
68	↓	C	↓	-1.822	27.5
69	↓	F	↓	-1.972	26.4
70	↓	F	↓	-2.028	26.1
71	↓	E	↓	-2.85	21.1
72	↓	F	9.07	0	40.0
73	3B	C	10.60	1.50	48.4
74	↓	F	↓	0	40.0
75	↓	C	↓	-.50	37.2
76	4B	C	12.31	1.50	47.5
77	↓	F	↓	0	40.0
78	↓	C	↓	-.50	37.5
79	1C	C	5.03	.50	84.5
80	↓	F	↓	0	80.0
81	↓	C	↓	-1.50	66.5
82	2C	E	7.80	2.50	97.2

[a] C - Corrugation
E - Edge
F - Flat
S - Support

TABLE II.- Continued

Thermocouple no.	Panel no.	Location on panel (a)	s/r	ℓ/d	β, deg
83	2C	C	7.80	0.50	83.4
84		F		0	80.0
85		F		-.972	73.3
86		F		-1.028	72.9
87		C		-1.178	71.8
88		C		-1.285	71.1
89		C		-1.392	70.4
90		C		-1.50	69.7
91		C		-1.608	69.0
92		C		-1.715	68.3
93		C		-1.822	67.5
94		F		-1.972	66.4
95		F		-2.028	66.1
96	3C	C	10.60	2.50	94.0
97		C		.50	82.8
98		F		0	80.0
99		C		-1.50	71.6
100	4C	C	12.31	2.50	92.5
101		C		.50	82.5
102		F		0	80.0
103		C		-1.50	72.5
104	1D	C	5.03	.50	124.5
105		F		0	120.0
106		C		-1.5	106.5
107	2D	C	7.80	.50	123.4
108		F		0	120.0
109		C		-1.50	109.7
110	3D	C	10.60	.50	122.8
111		F		0	120.0
112		C		-1.50	111.6
113	4D	C	12.31	.50	122.5
114		F		0	120.0
115		C		-1.50	112.5
116	1E	F	5.03	0	160.0
117	2E	F	7.80	0	160.0
118	3E	F	10.60	0	160.0
119	1F	F	5.03	0	-160.0
120	2F	F	7.80	0	-160.0
121	3F	F	10.60	0	-160.0
122	1G	F	5.03	0	-120.0
123	2G	F	7.80	0	-120.0
124	3G	F	10.60	0	-120.0

[a] C - Corrugation
E - Edge
F - Flat
S - Support

TABLE II.- Concluded

Thermocouple no.	Panel no.	Location on panel (a)	s/r	ℓ/d	β, deg
125	1H	F	5.03	0	-80.0
126	2H	F	7.80	0	-80.0
127	3H	F	10.60	0	-80.0
128	1I	F	5.03	0	-40.0
129	2I	F	7.80	0	-40.0
130	3I	F	10.60	0	-40.0
131	4I	F	12.31	0	-40.0

[a] C - Corrugation
E - Edge
F - Flat
S - Support

TABLE III.- TEST CONDITIONS

Test	T_t, K	q_∞, kPa	α, deg	M_∞	R_∞, per meter	p_s, kPa	$\dot{q}_s$, MW/m^2
[a]1	1867	64.6	0.0	6.64	4.76×10^6	124.1	0.62
High Reynolds number							
2	1862	61.0	0.0	6.76	4.38×10^6	115.8	0.59
3	1802	62.7	.0	6.68	4.58	116.5	.58
4	1708	62.6	5.0	6.51	4.73	115.3	.53
5	1981	60.4	9.9	6.90	4.21	113.9	.65
Low Reynolds number							
6	1981	24.3	0.0	7.17	1.86×10^6	46.3	0.42
7	1746	24.6	0.0	6.78	2.02	47.1	.35
8	1908	25.9	0.3	7.06	1.87	46.7	.40
9	1779	24.8	5.0	6.83	2.00	47.3	.36
10	1752	24.1	10.0	6.78	2.01	47.1	.35
11	1900	24.8	10.0	7.06	1.85	46.4	.40

[a]Smooth-cone data

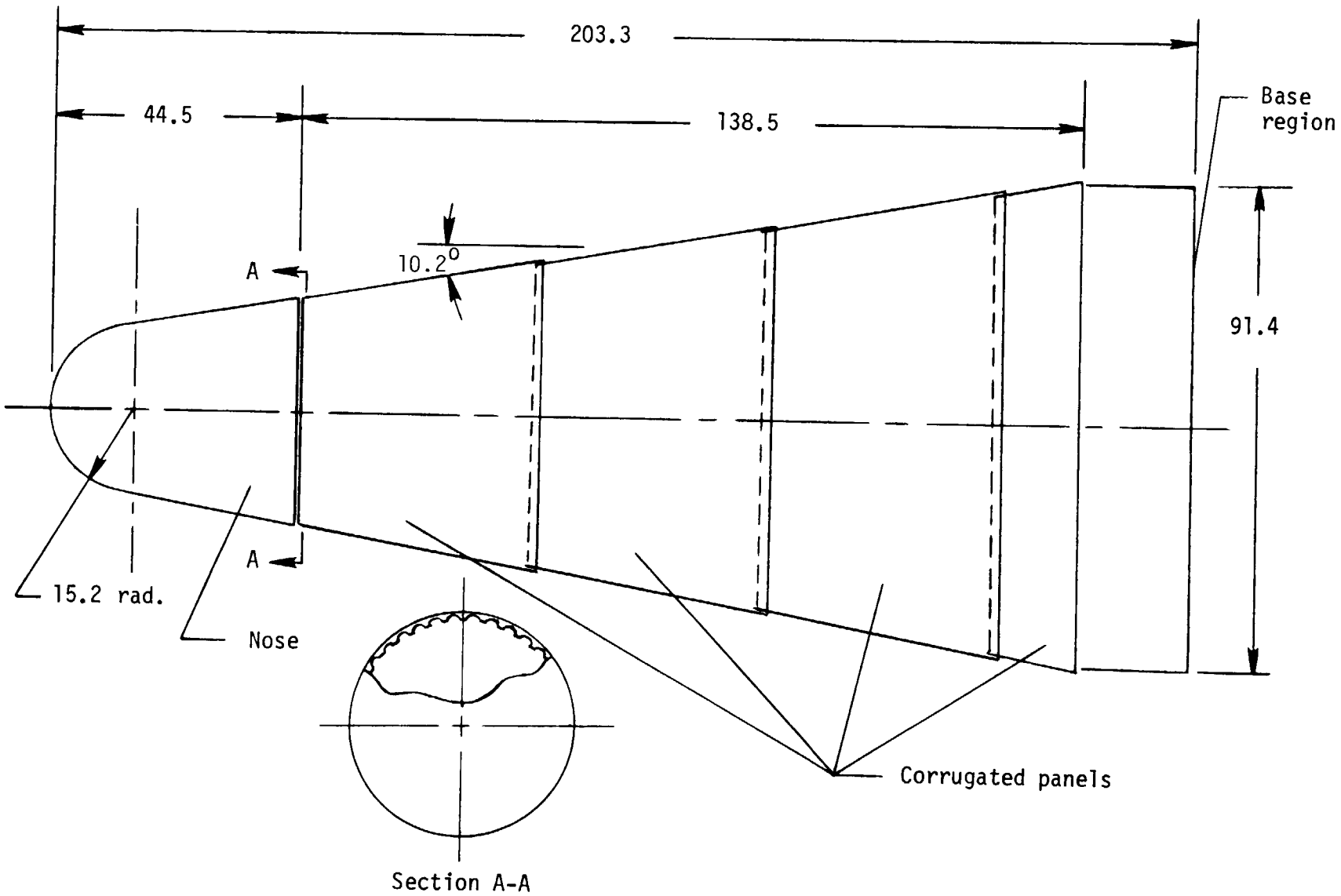

Figure 1.- Schematic of 10.2° blunted-cone model. All linear dimensions are in cm.

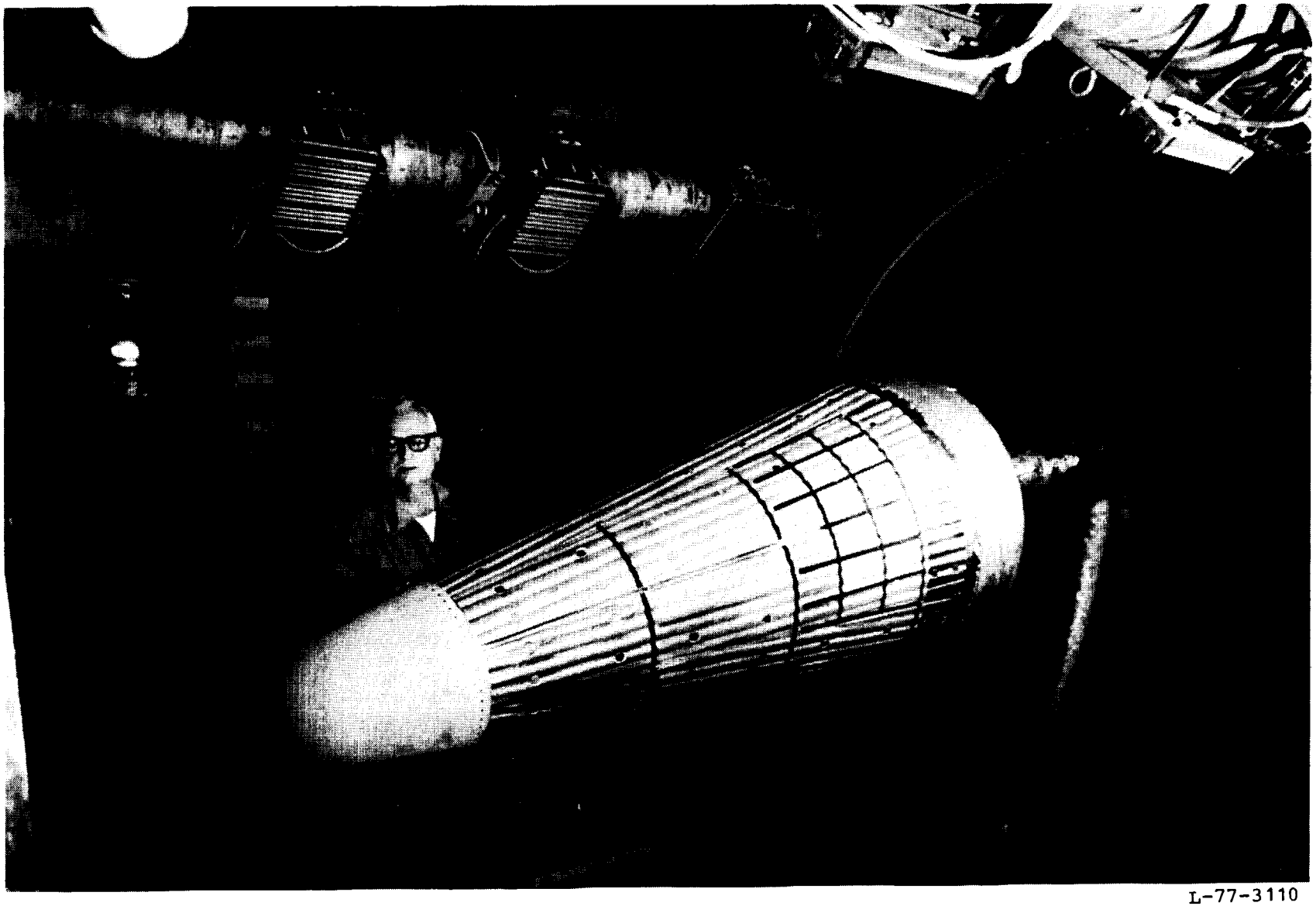

L-77-3110

Figure 2.- 10.2° blunted-cone model mounted on sting in Langley 8-Foot High-Temperature Structures Tunnel.

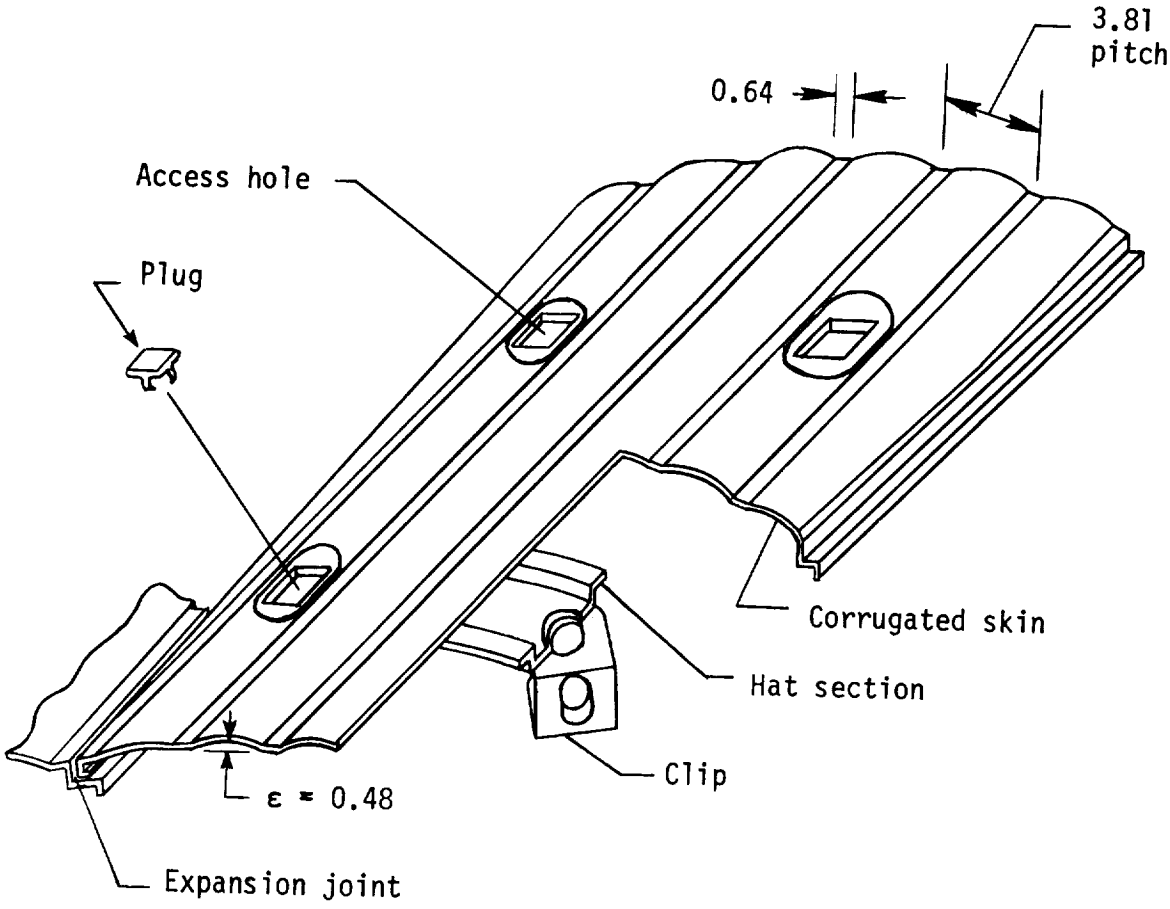

Figure 3.- Typical corrugated curved metallic panel. All dimensions are in cm.

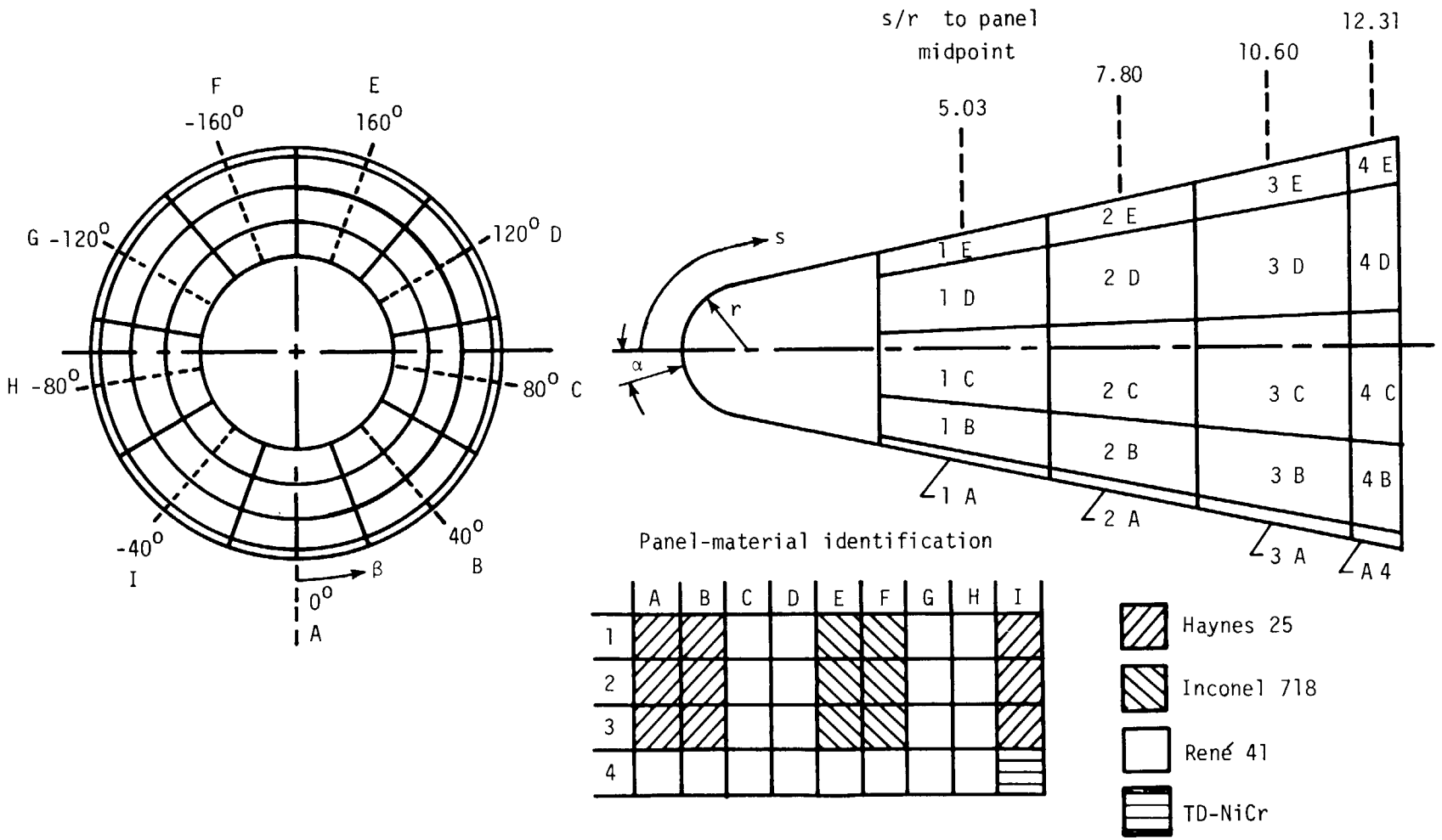

Figure 4.- Panel and material identification.

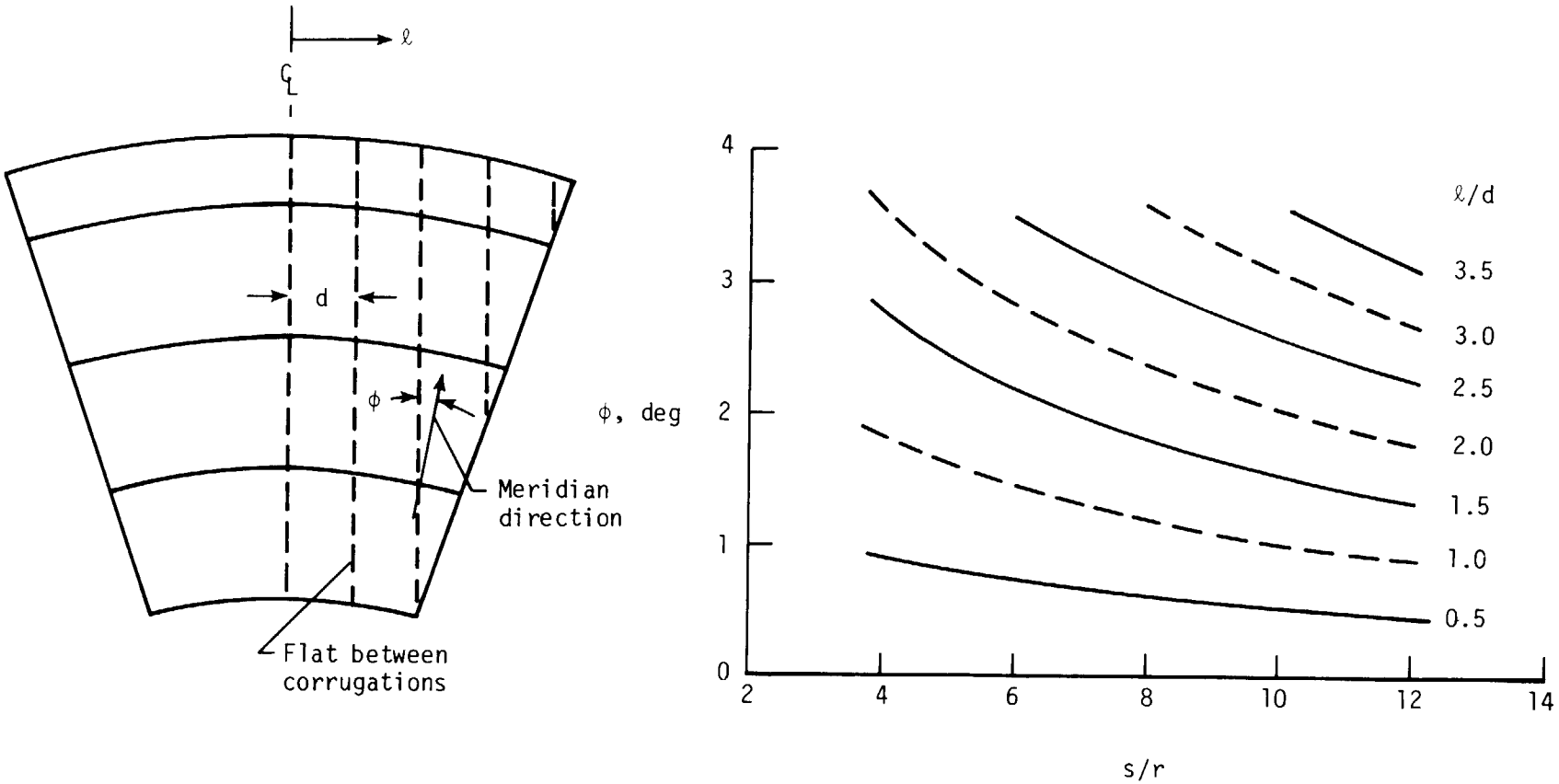

Figure 5.- Local corrugation angles for the flats and crests.

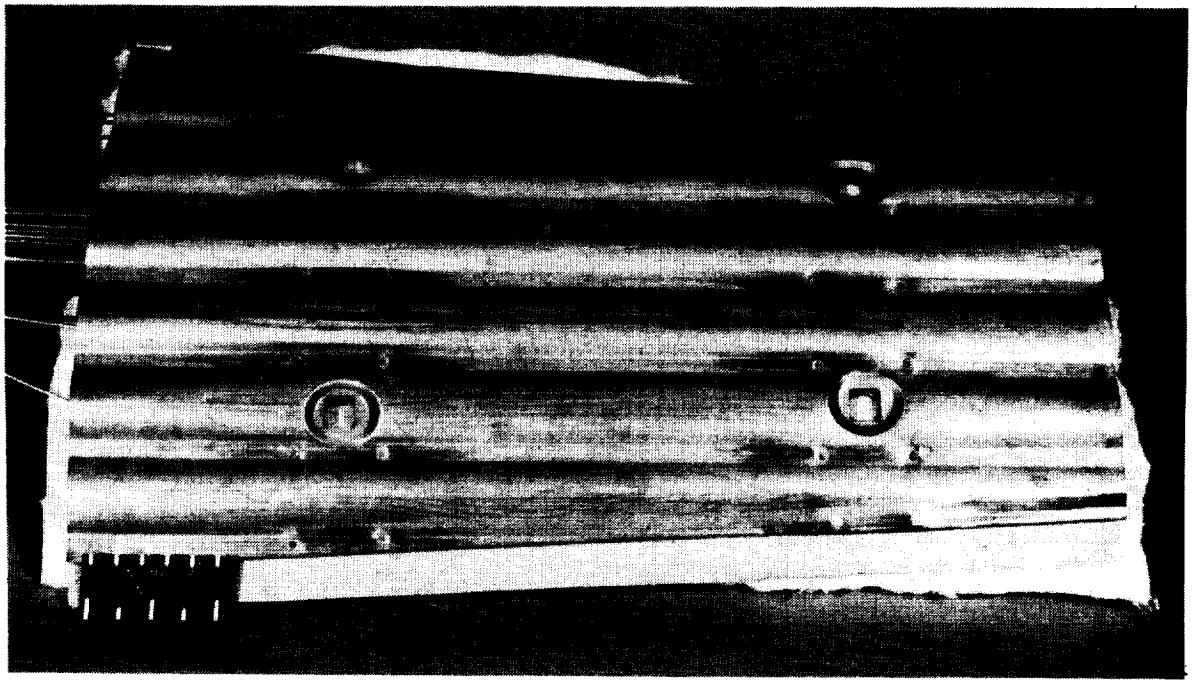

(a) Panel top surface.

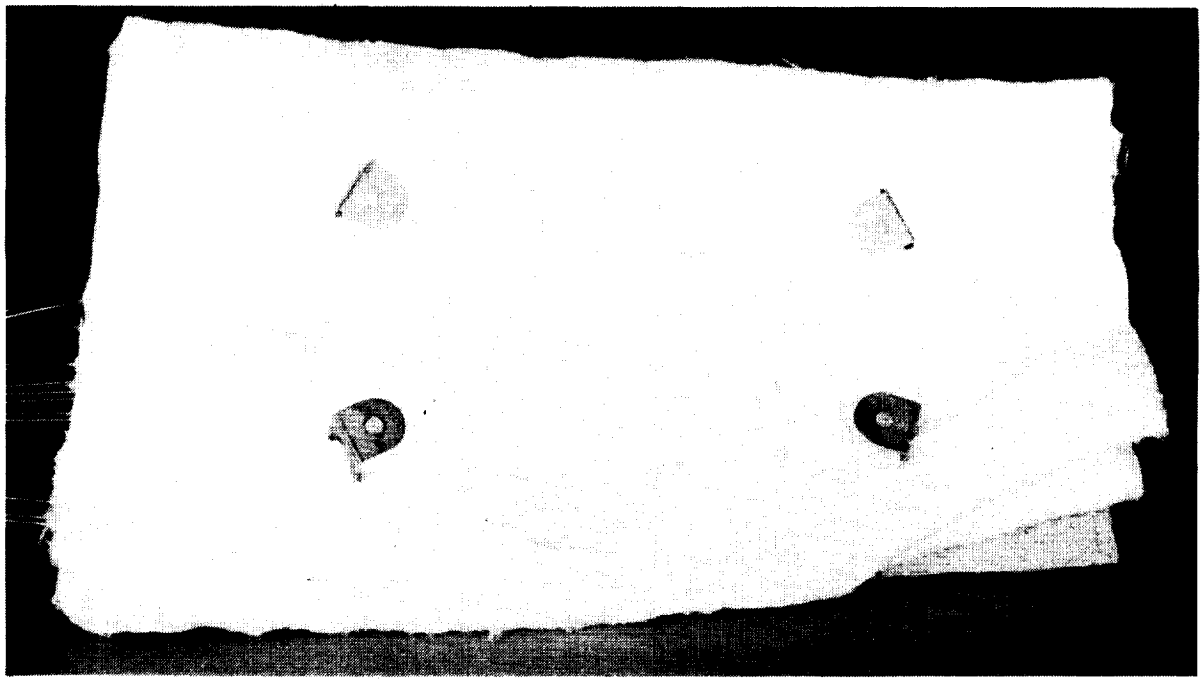

(b) Panel bottom surface with insulation.

L-77-799

Figure 6.- Typical corrugated panel with insulation.

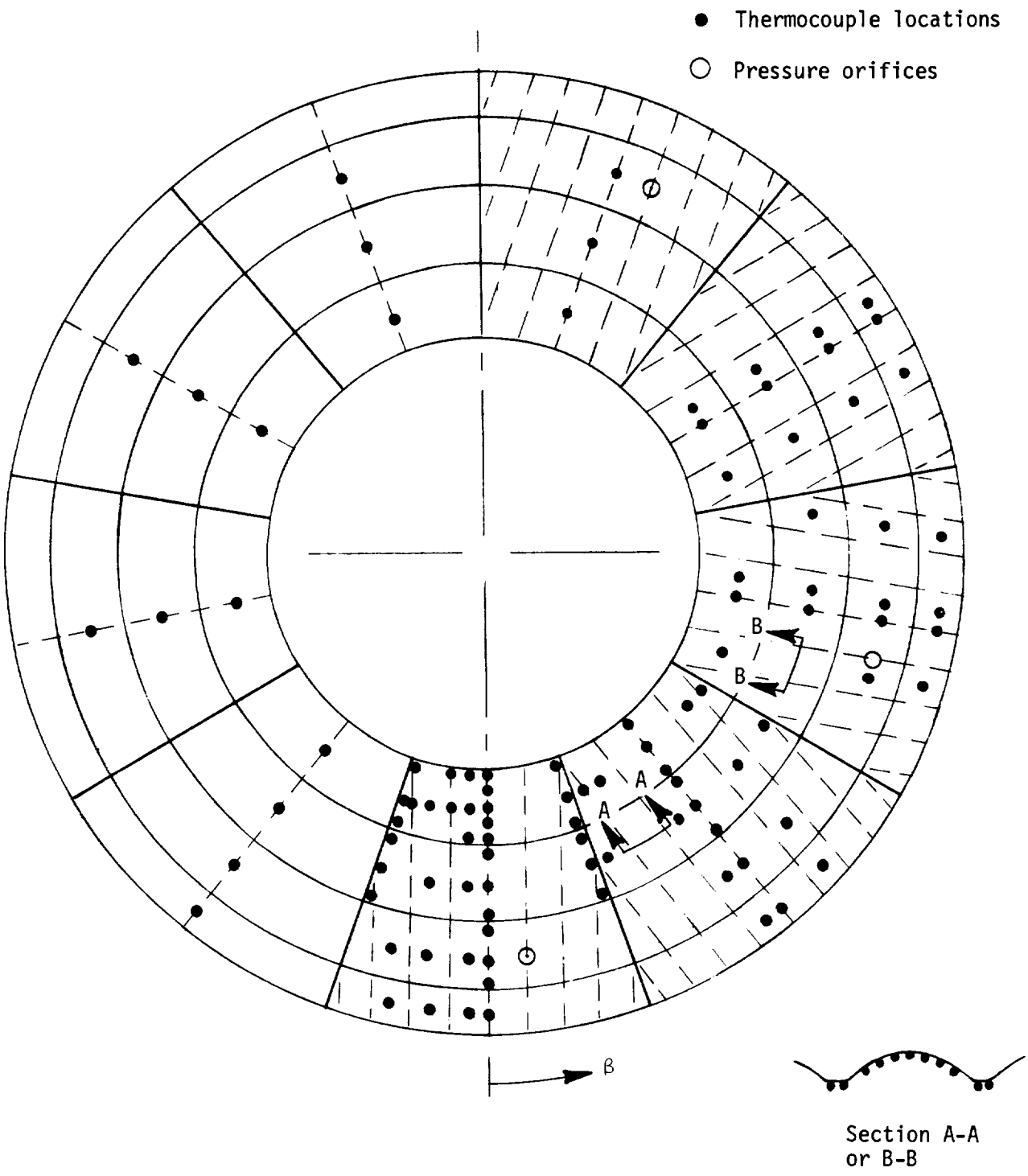

Figure 7.- Thermocouple and pressure-orifice locations.

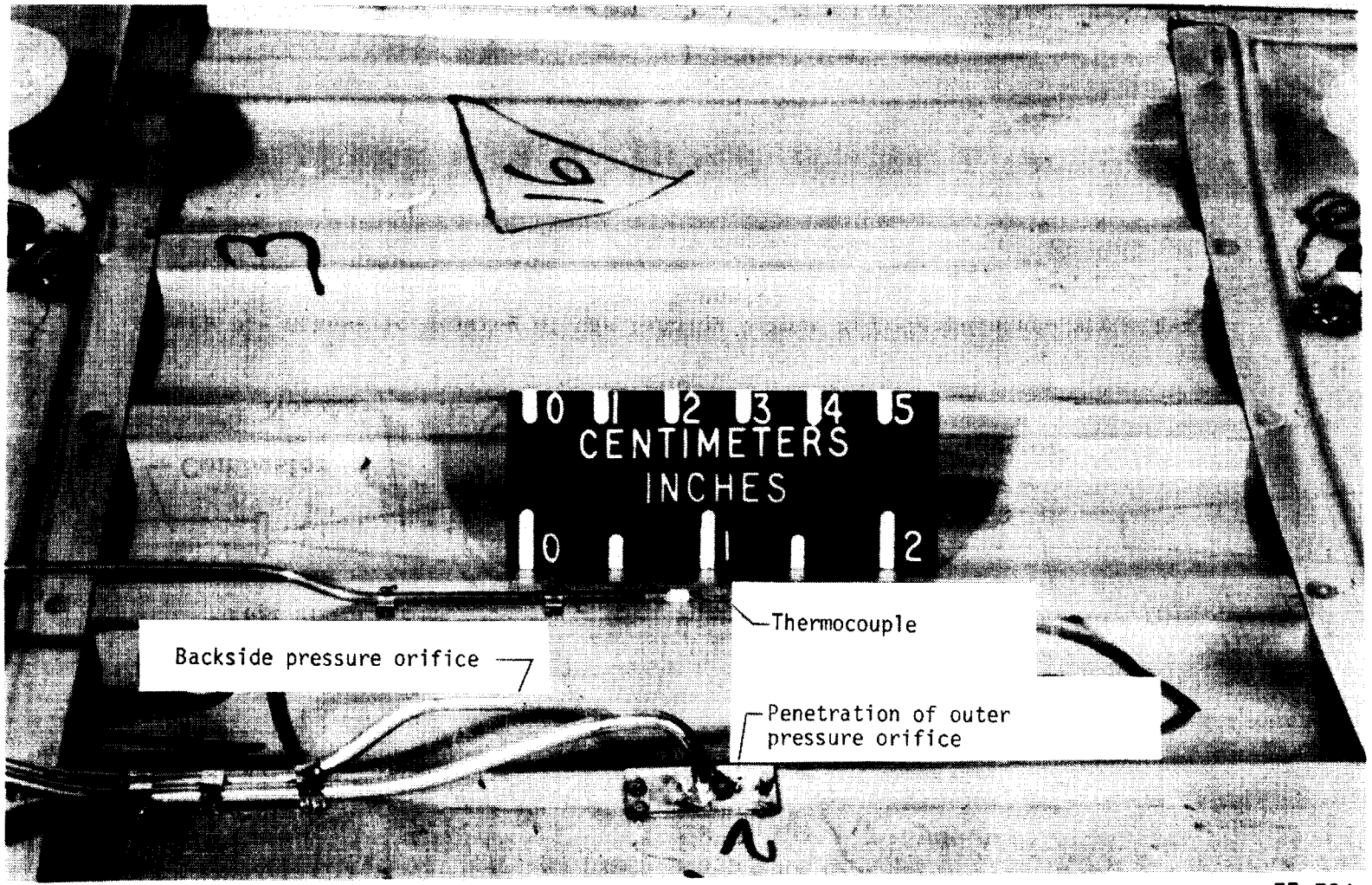

L-77-794

Figure 8.- Typical panel thermocouple and pressure tube installation.

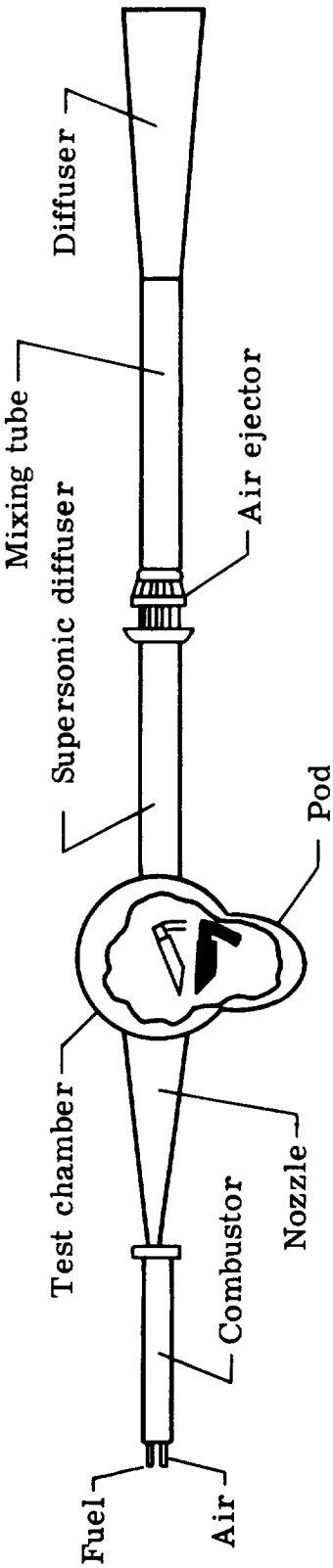

Figure 9.- Schematic drawing of the Langley 8-Foot High-Temperature Structures Tunnel.

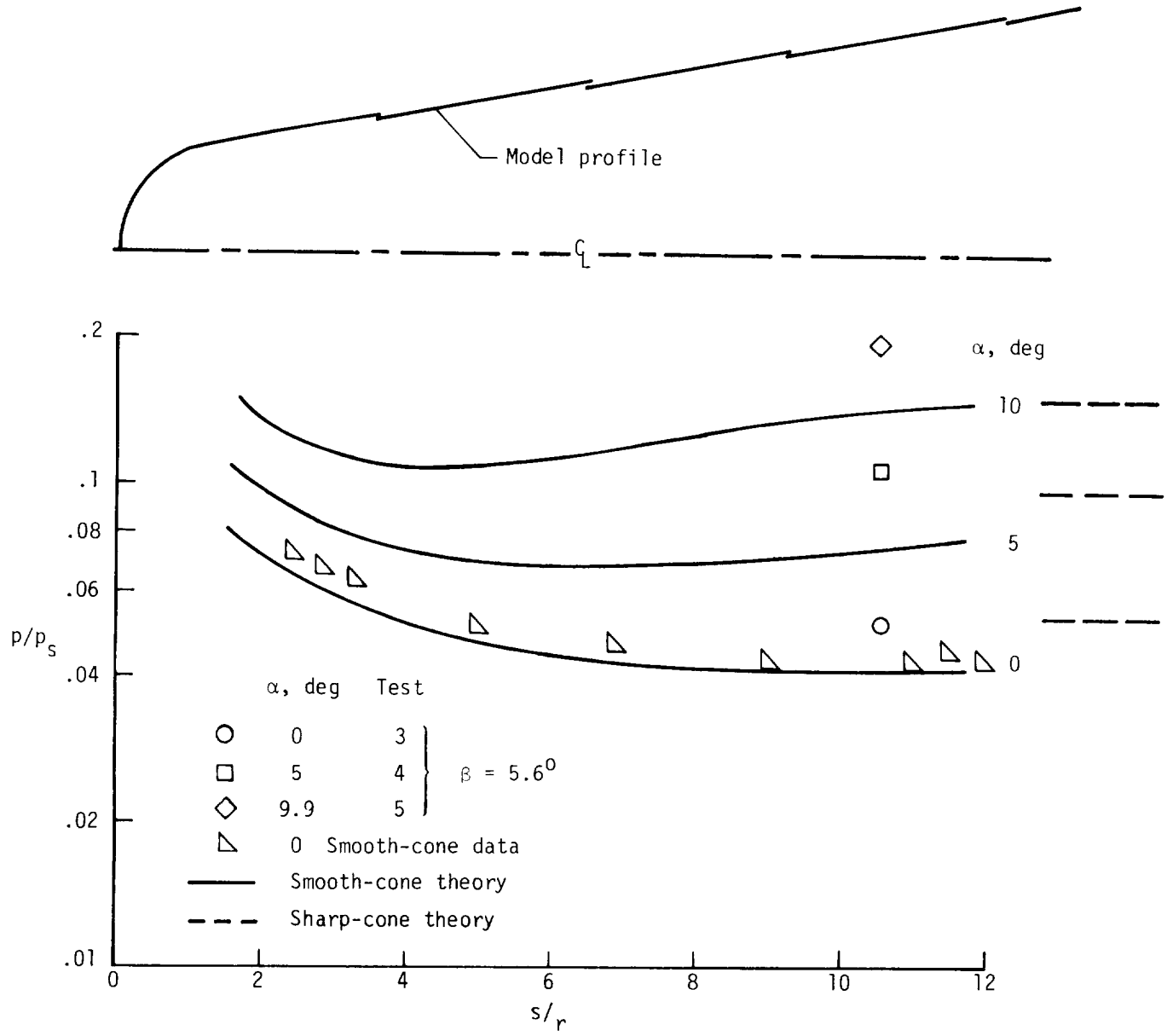

Figure 10.- Longitudinal pressure distributions along windward meridian.

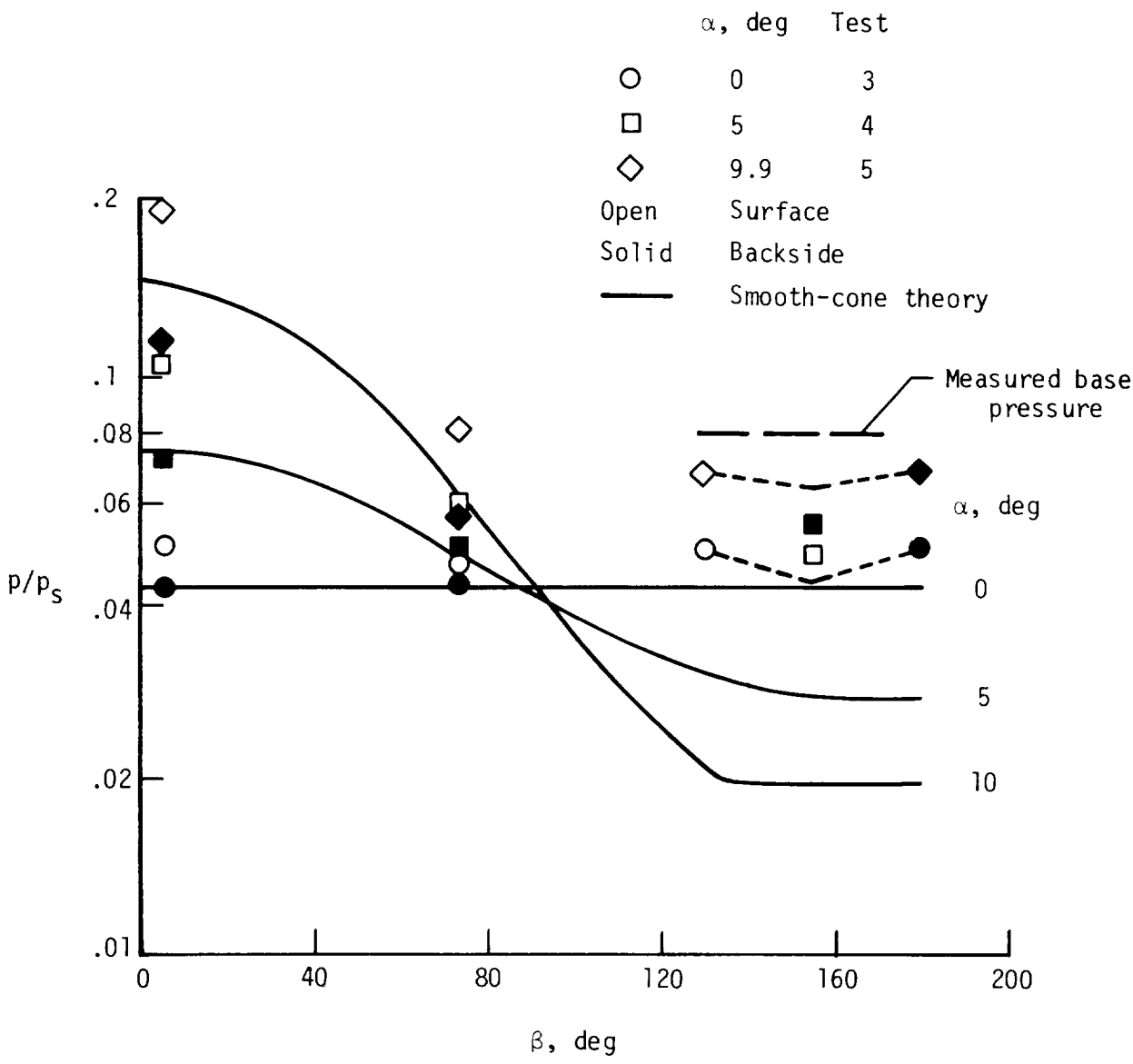

Figure 11.- Circumferential pressure distributions at s/r = 10.6.

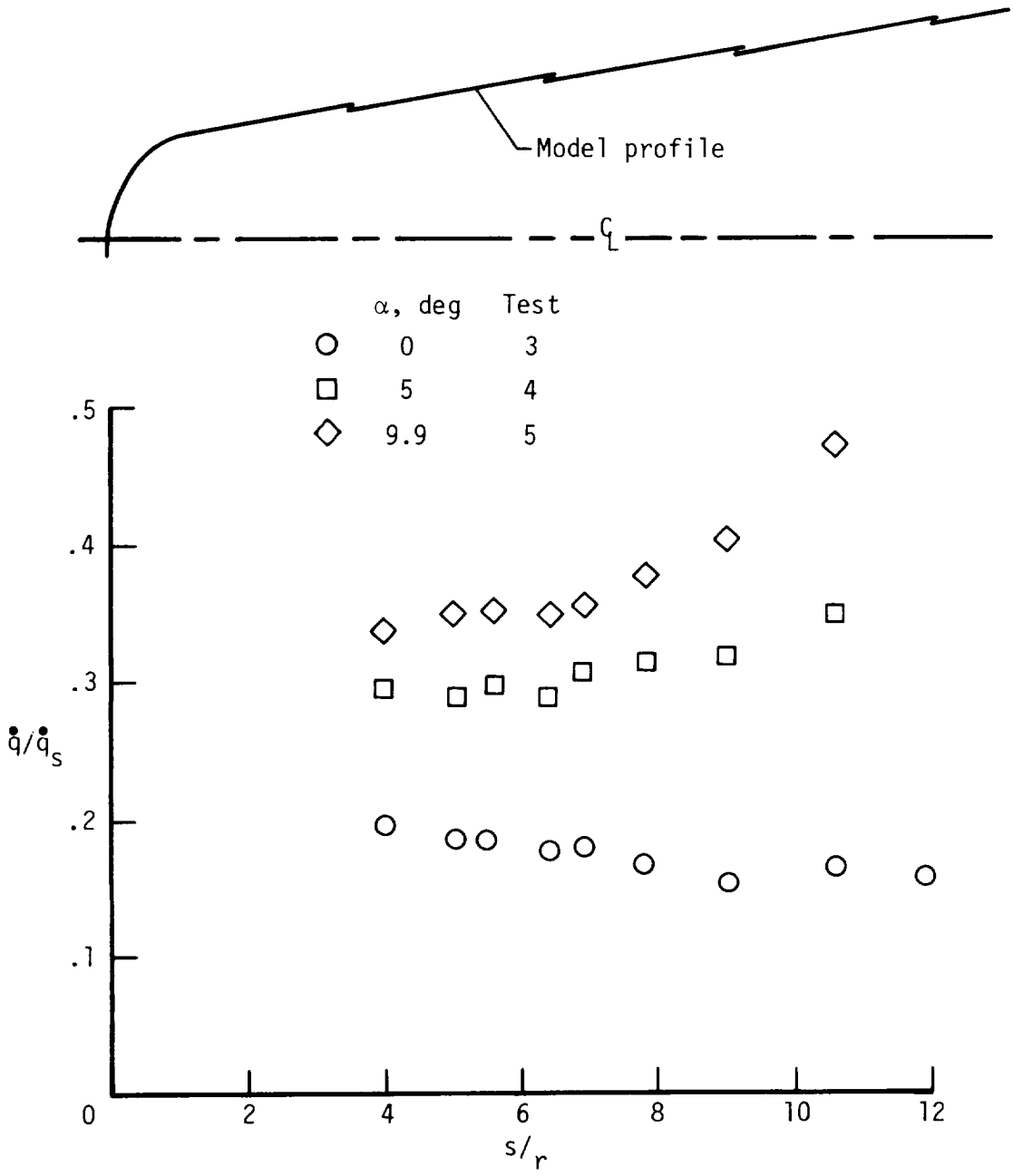

Figure 12.- Effect of angle of attack on longitudinal heating-rate distributions along windward meridian.

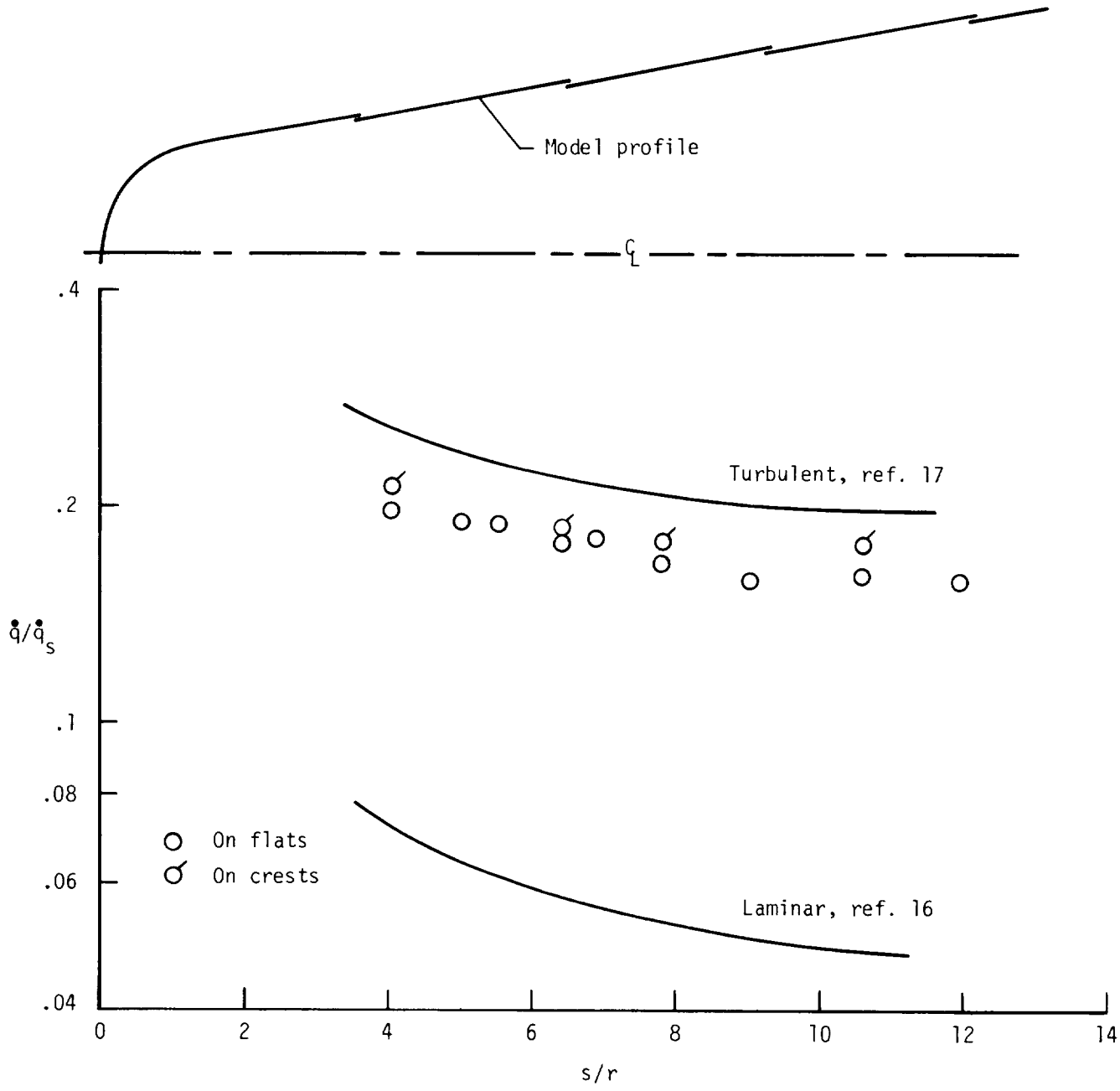

(a) $\alpha = 0°$.

Figure 13.- Comparison of longitudinal heating on corrugation flats and crests with theory along windward meridian.

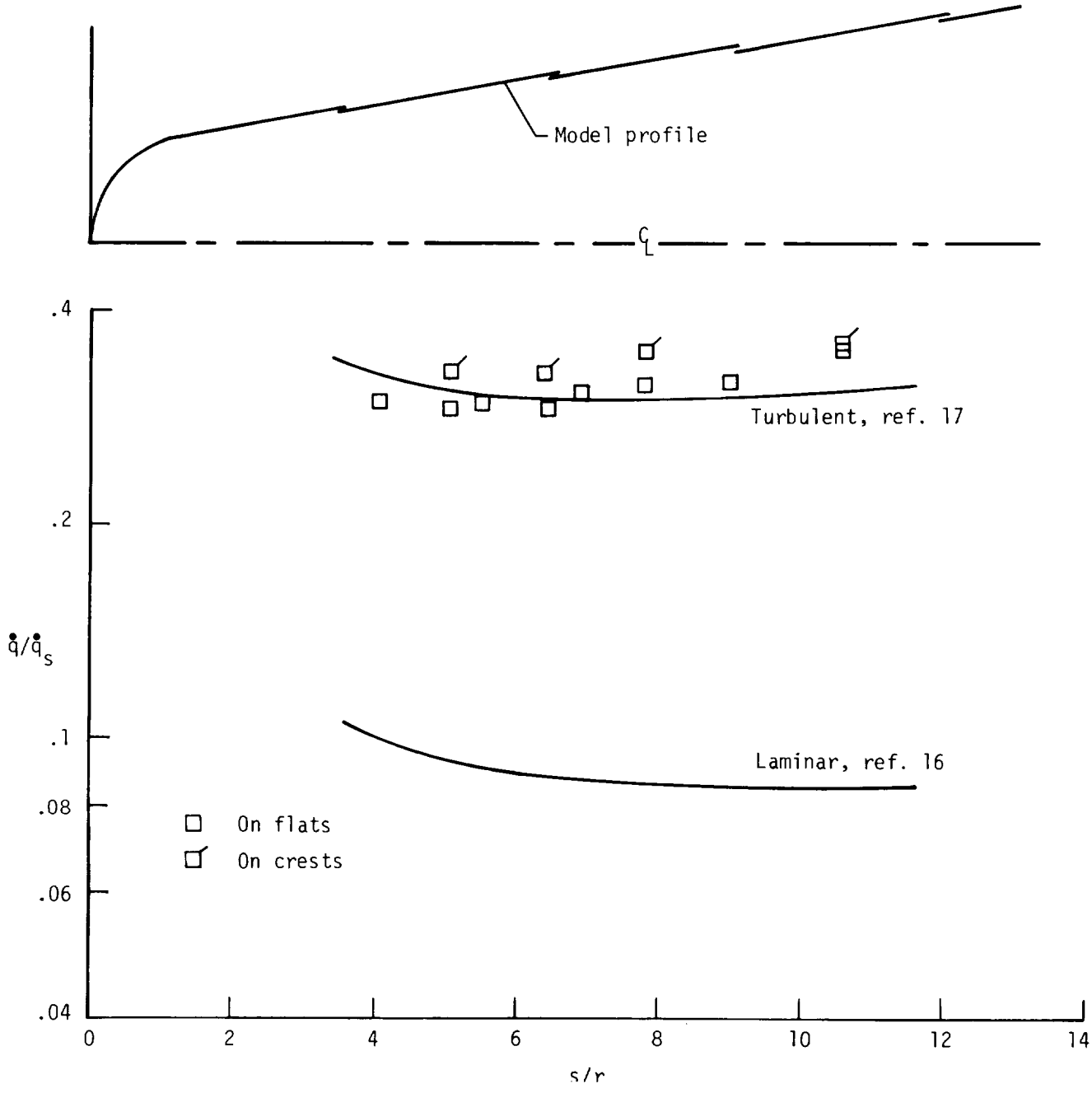

(b) $\alpha = 5°$.

Figure 13.- Continued.

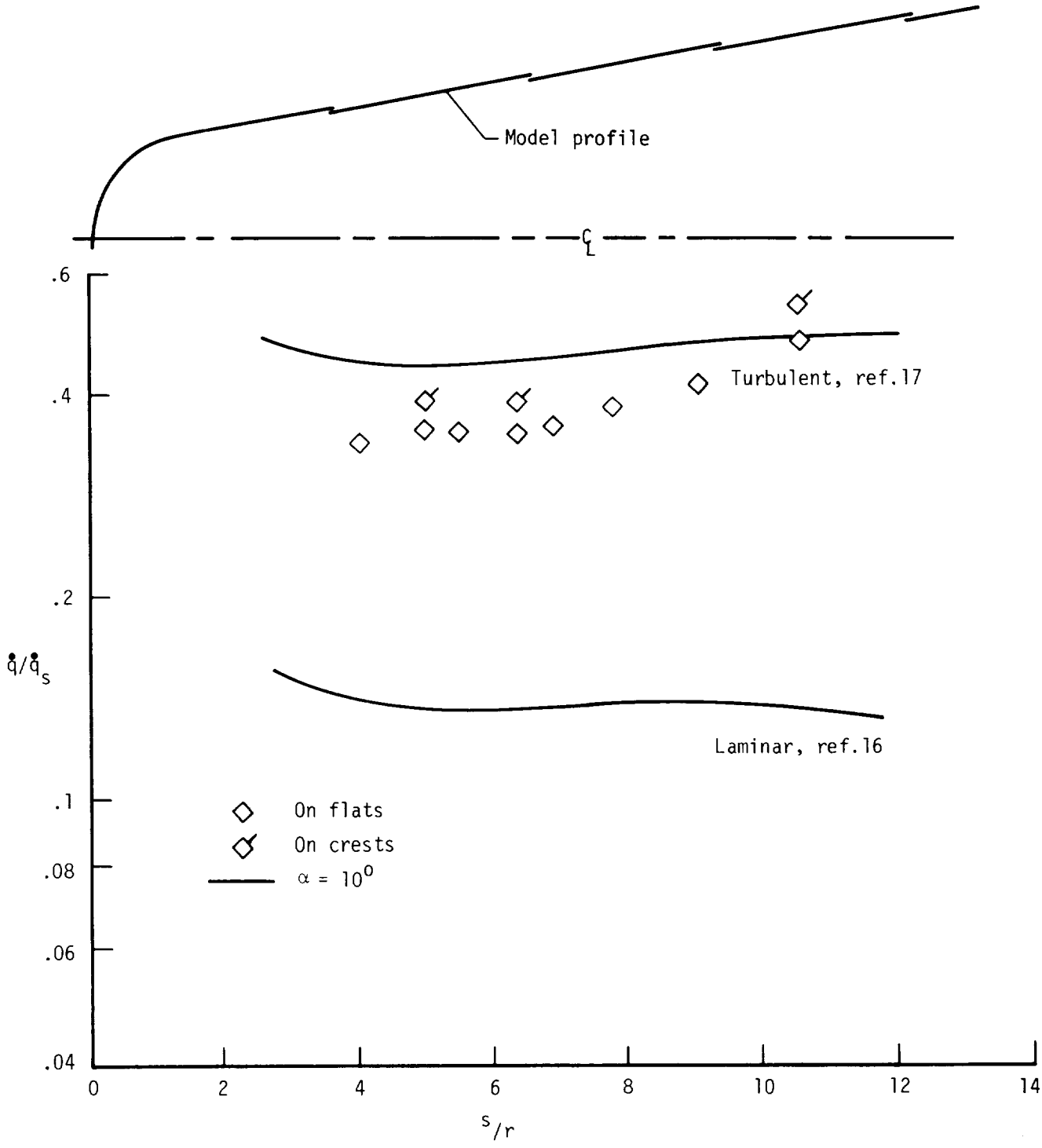

(c) $\alpha = 9.9°$.

Figure 13.- Concluded.

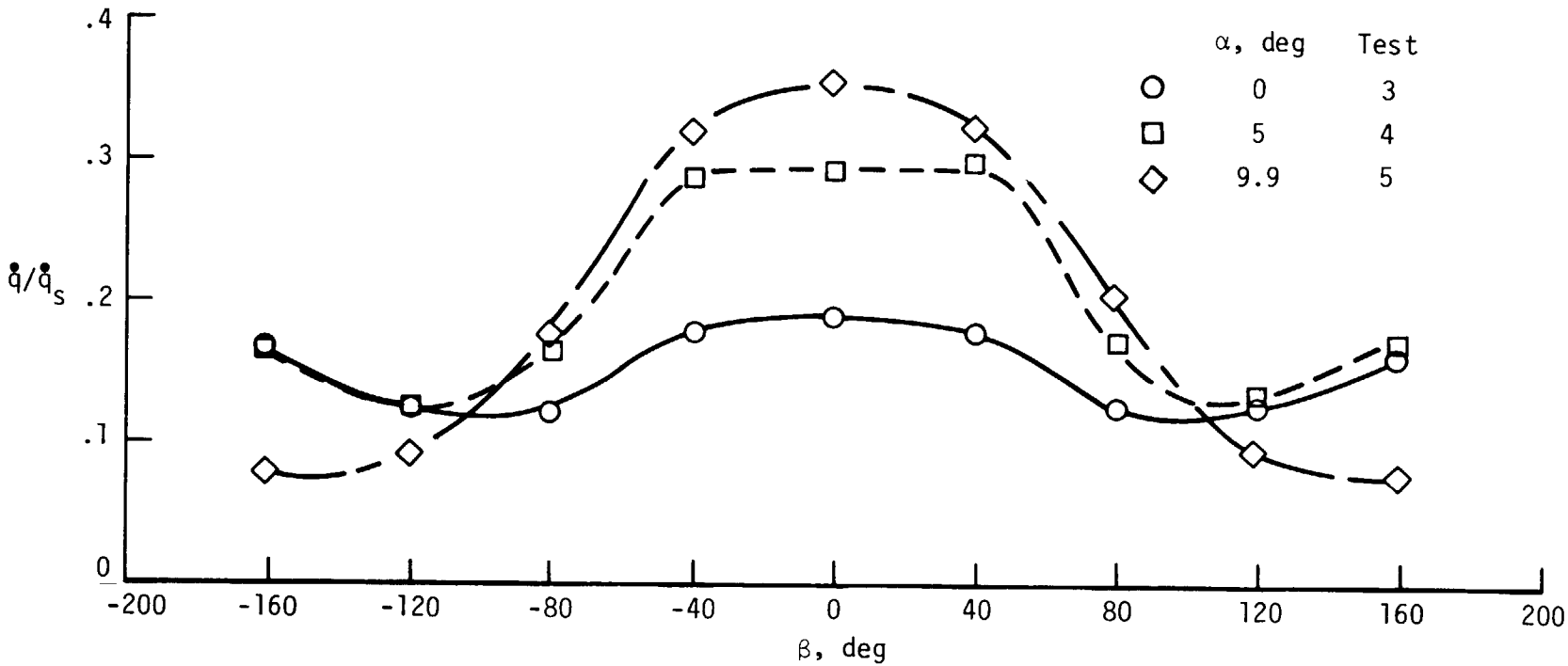

(a) s/r = 5.03.

Figure 14.- Circumferential heating-rate distributions.

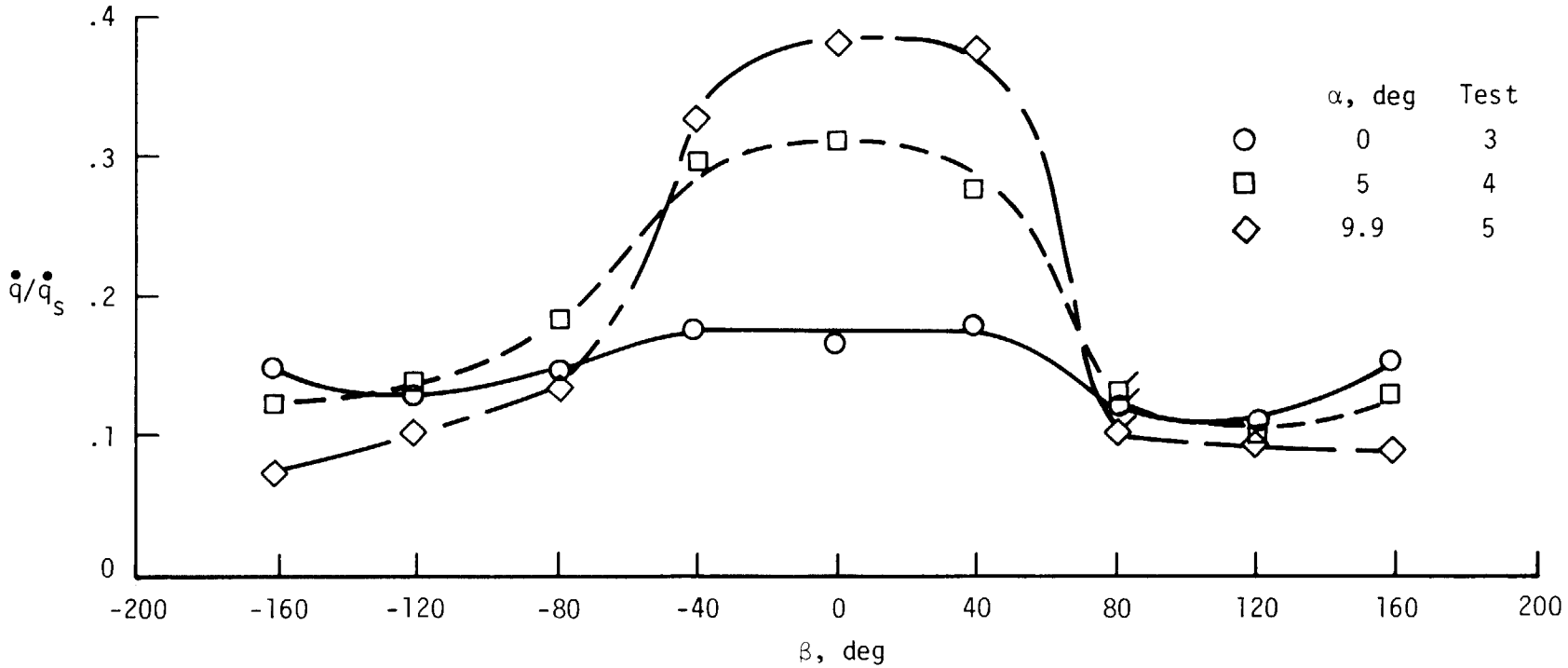

(b) s/r = 7.80.

Figure 14.- Continued.

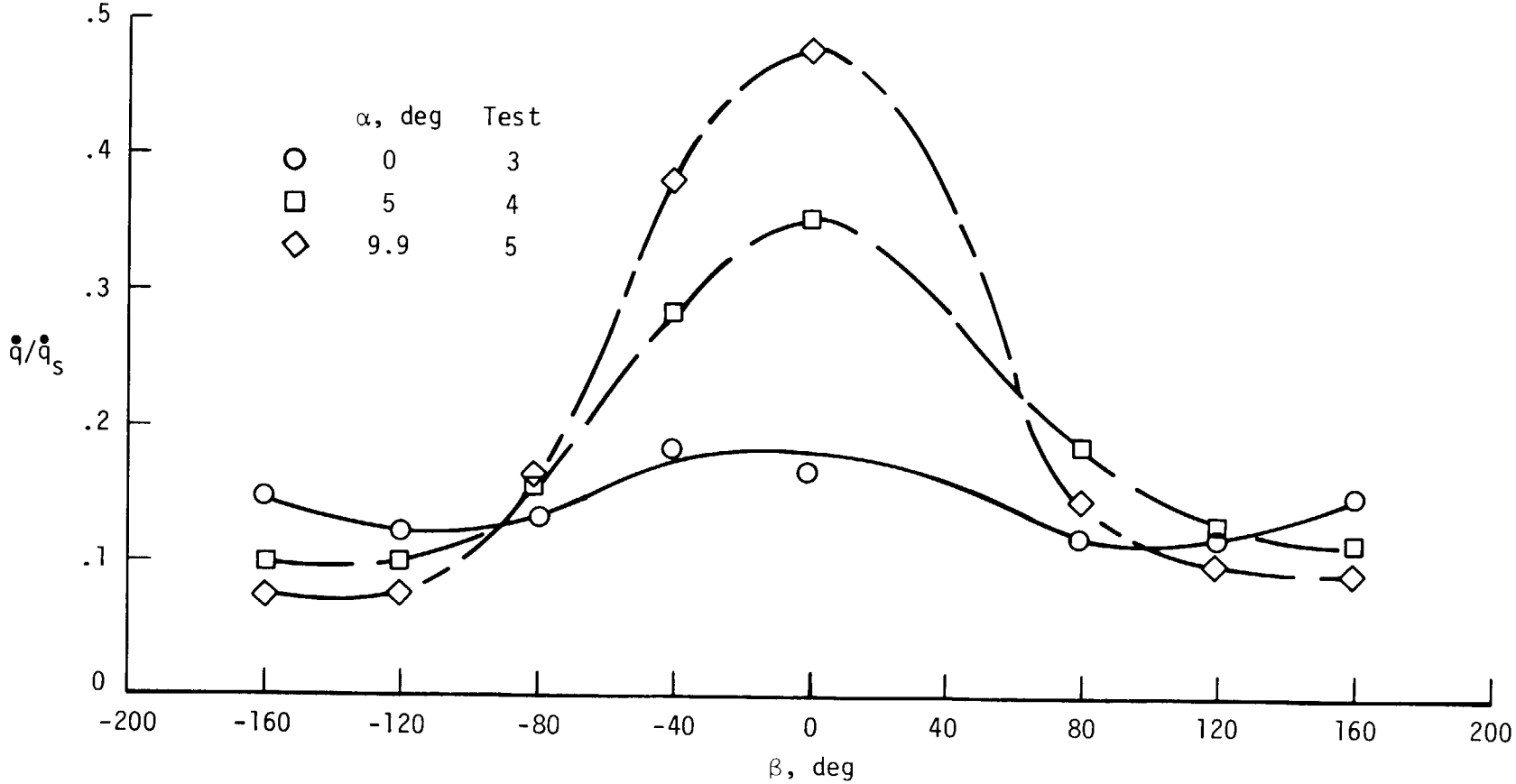

(c) s/r = 10.60.

Figure 14.- Concluded.

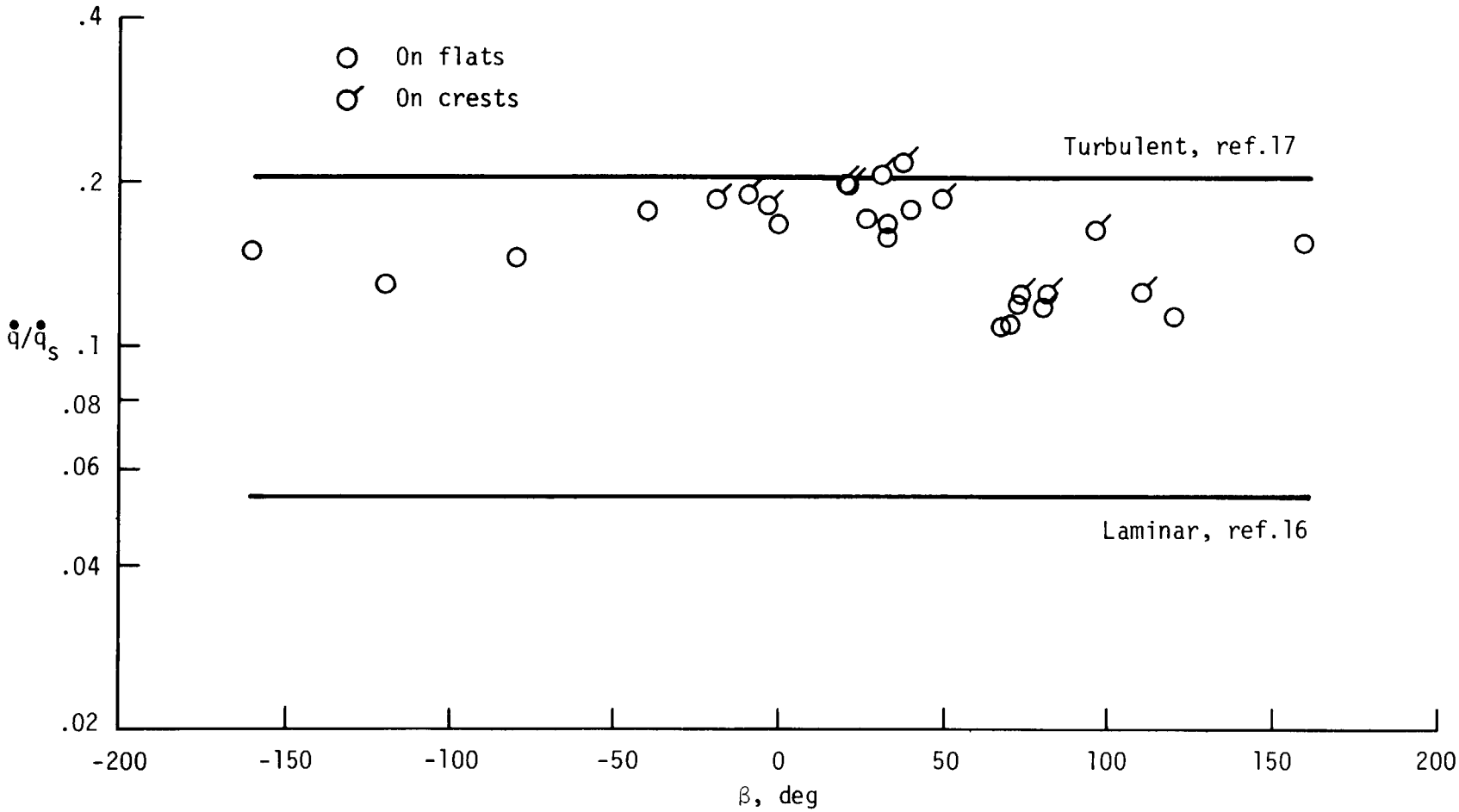

(a) $\alpha = 0°$.

Figure 15.- Circumferential heating distributions at s/r = 7.80.

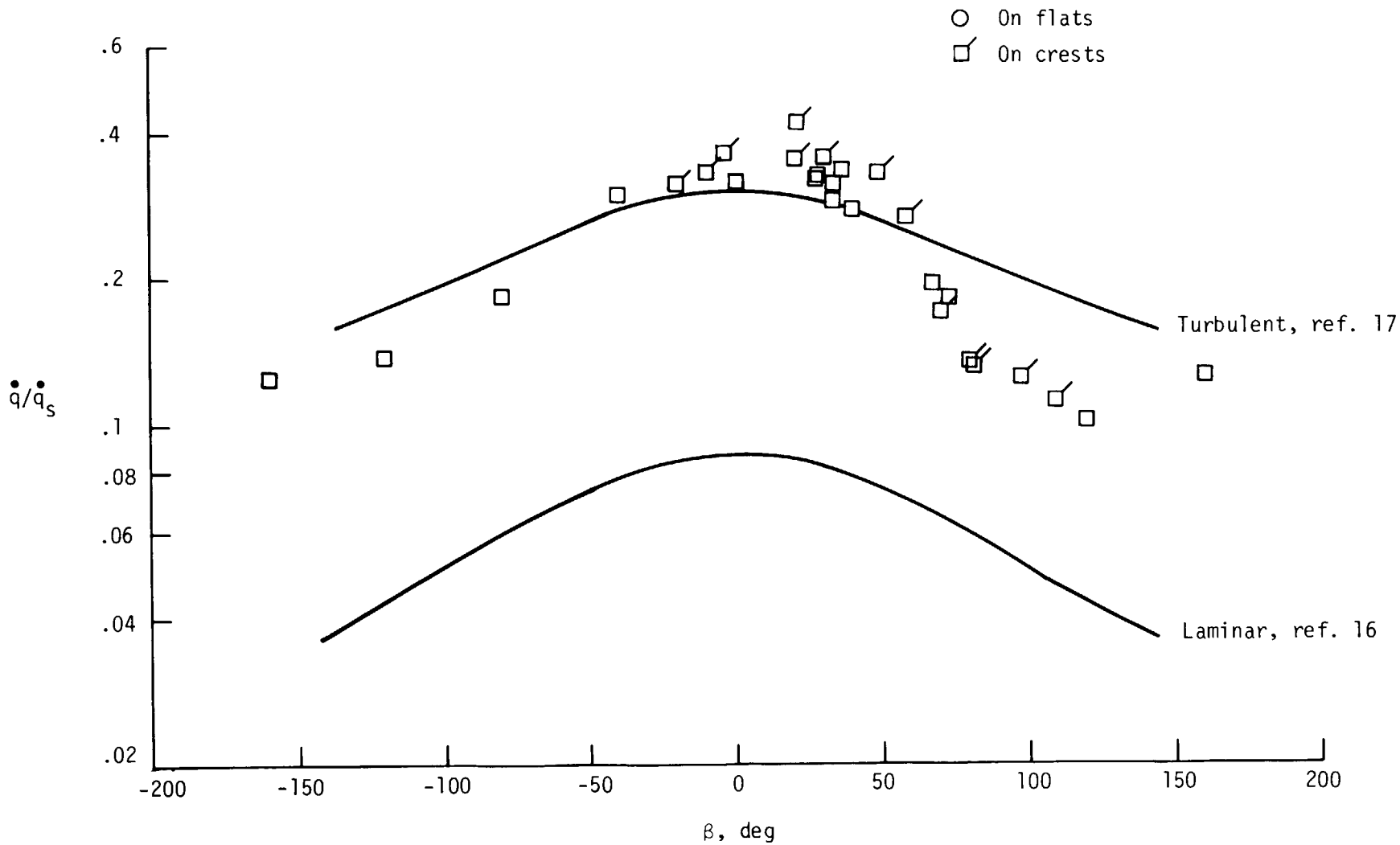

(b) $\alpha = 5°$.

Figure 15.- Continued.

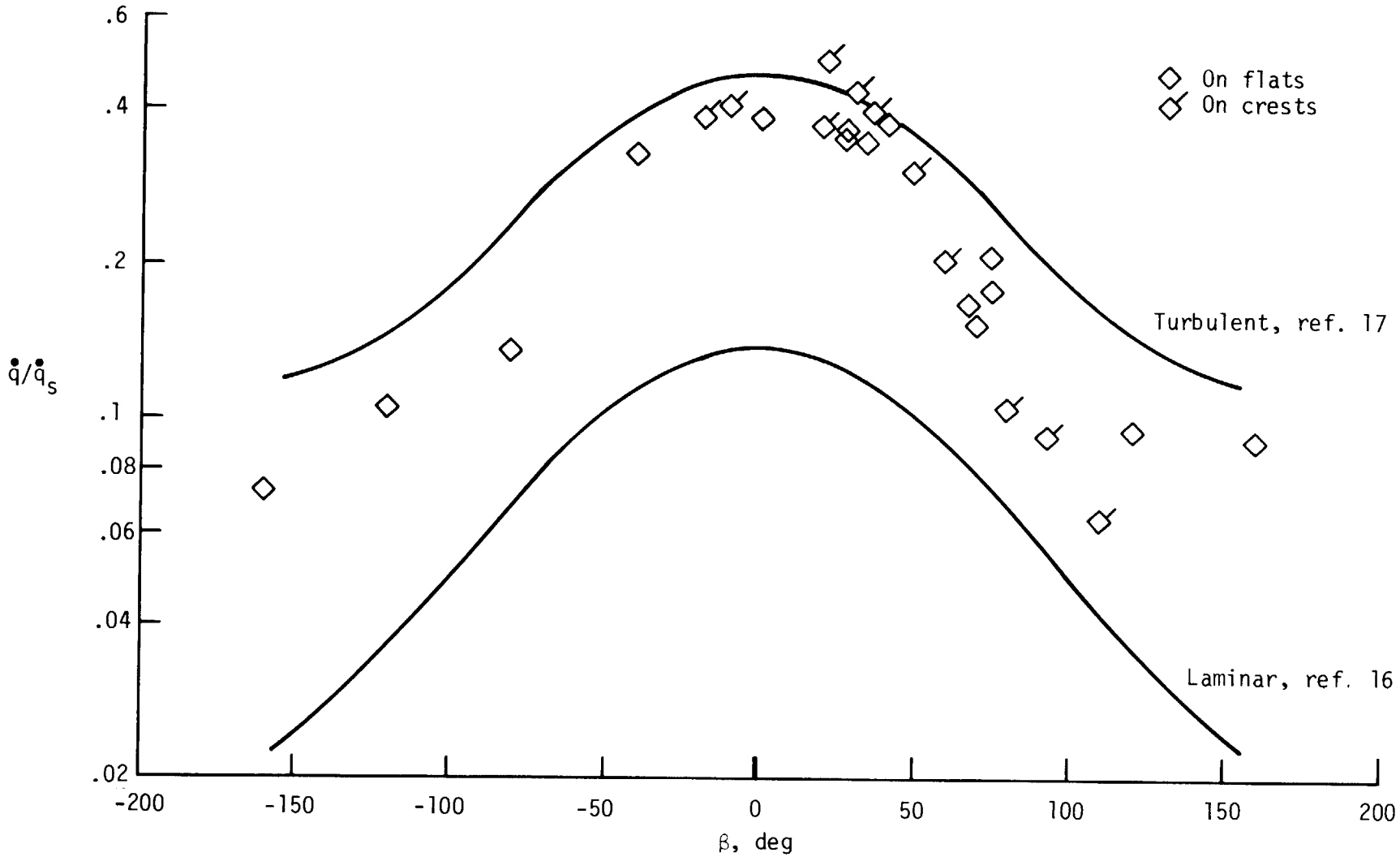

(c) $\alpha = 9.9°$.

Figure 15.- Concluded.

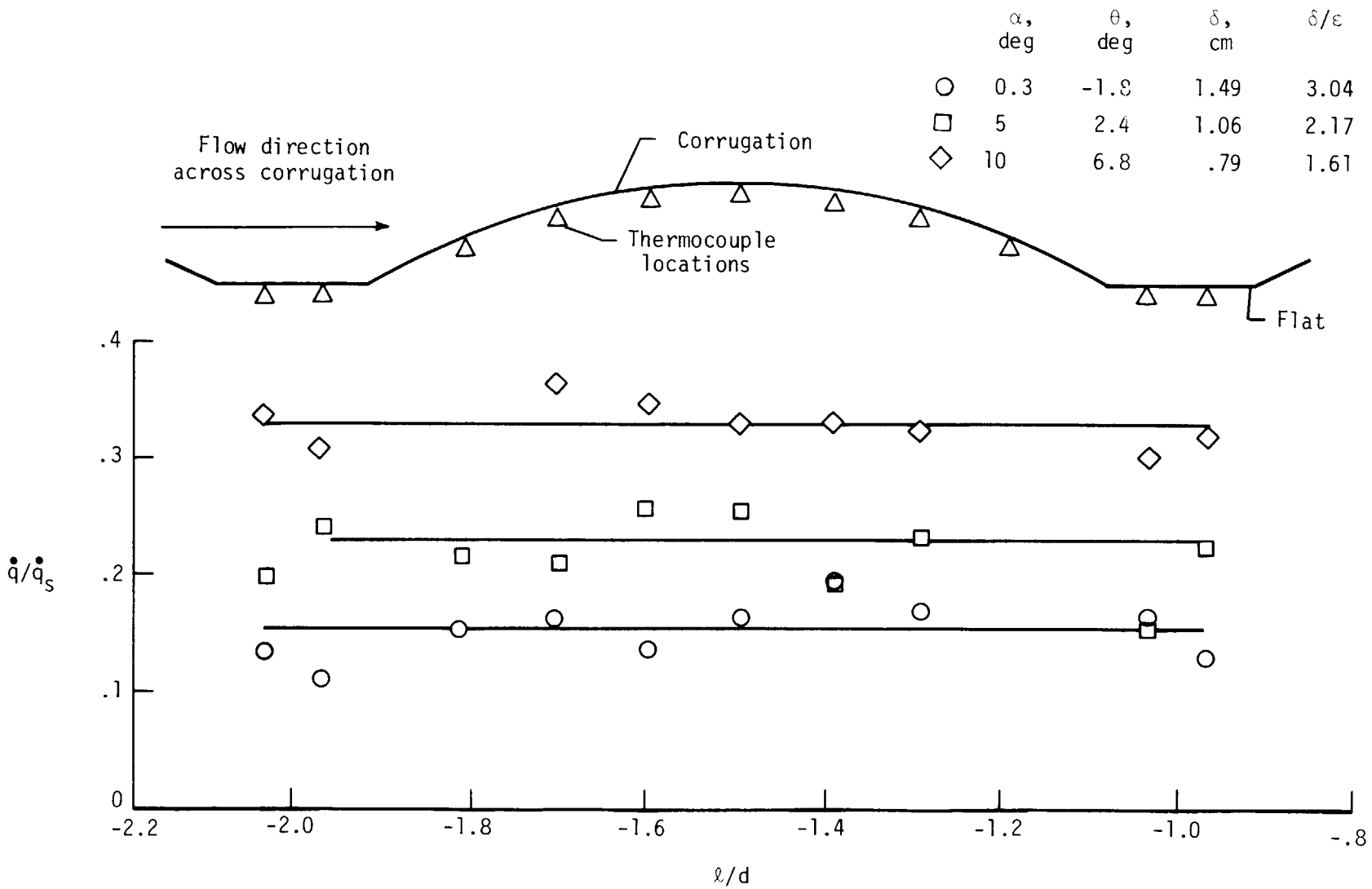

(a) Low Reynolds number range.

Figure 16.- Heating-rate distributions across corrugations at $\beta = 30°$ and $s/r = 7.80$ on panel 2B.

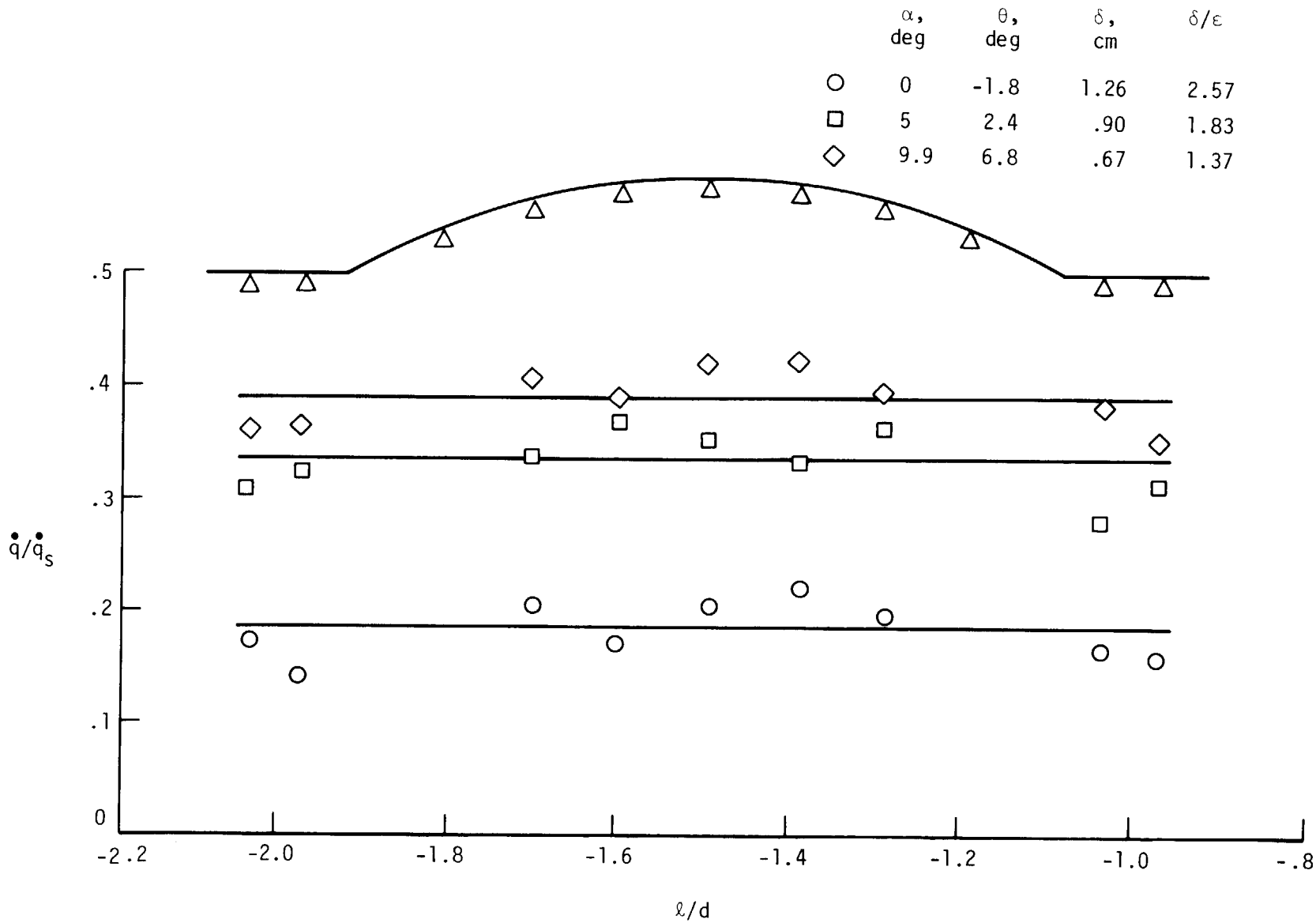

(b) High Reynolds number range.

Figure 16.- Concluded.

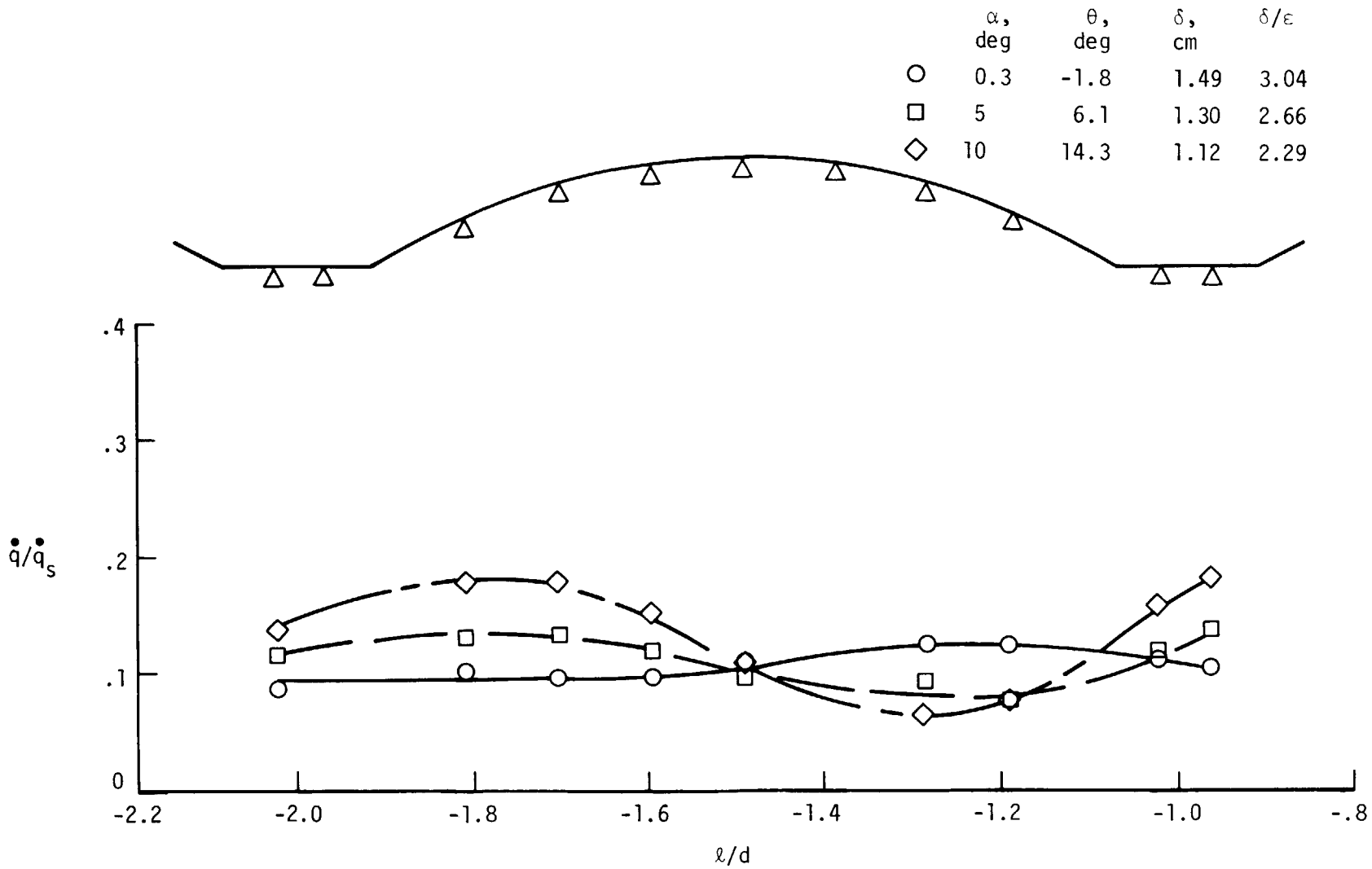

(a) Low Reynolds number range.

Figure 17.- Heating-rate distributions across corrugations at $\beta = 70°$ and $s/r = 7.80$ on panel 2C.

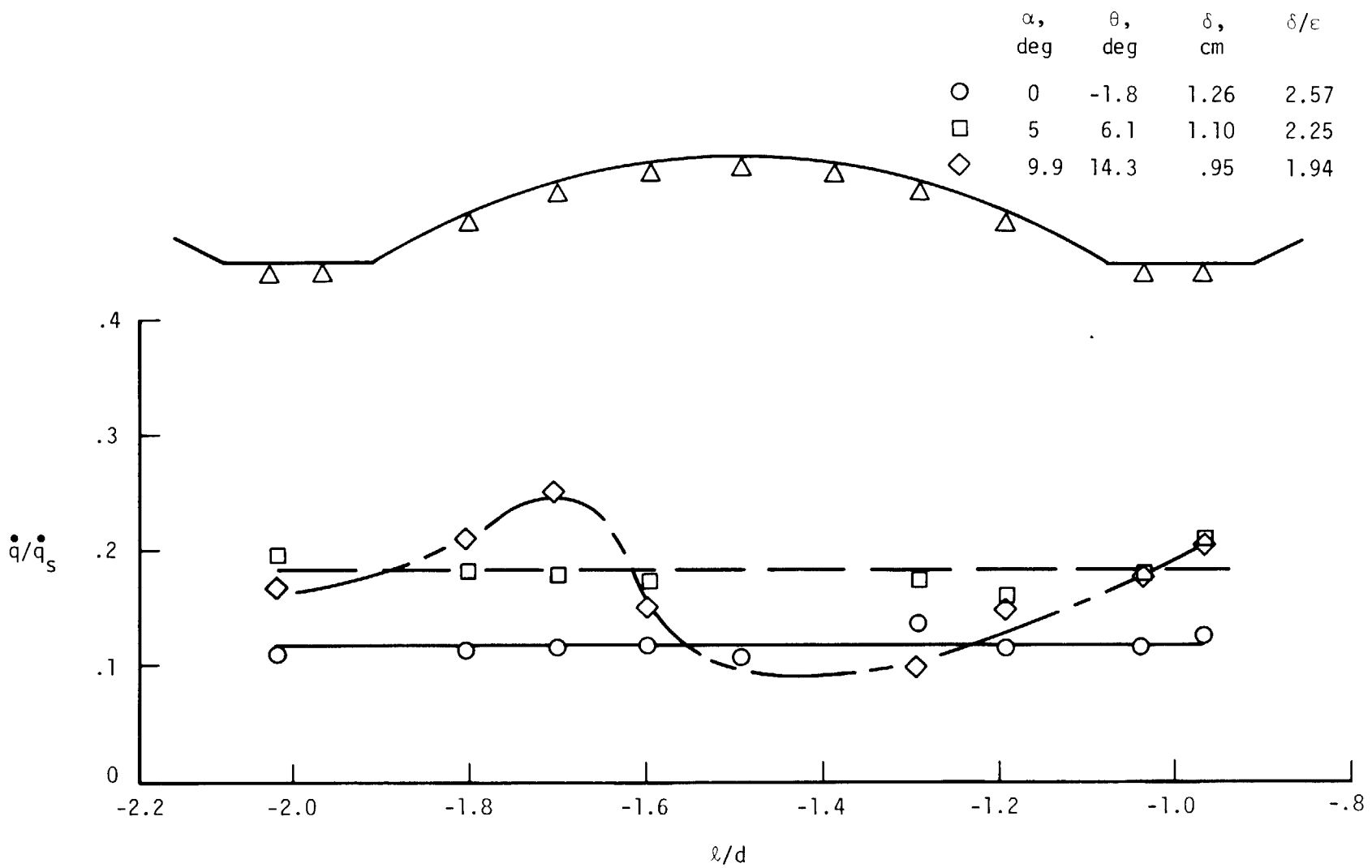

(b) High Reynolds number range.

Figure 17.- Concluded.

1. Report No.	2. Government Accession No.	3. Recipient's Catalog No.
NASA TP-1928		

4. Title and Subtitle	5. Report Date
AERODYNAMIC HEATING ON THE CORRUGATED SURFACE OF A 10.2° HALF-ANGLE BLUNTED CONE AT MACH 6.7	December 1981
	6. Performing Organization Code 506-53-63-05
7. Author(s) Irving Weinstein, Don E. Avery, and L. Roane Hunt	8. Performing Organization Report No. L-14679
9. Performing Organization Name and Address NASA Langley Research Center Hampton, VA 23665	10. Work Unit No.
	11. Contract or Grant No.
12. Sponsoring Agency Name and Address National Aeronautics and Space Administration Washington, DC 20546	13. Type of Report and Period Covered Technical Paper
	14. Sponsoring Agency Code

15. Supplementary Notes

16. Abstract

A 10.2° half-angle blunted cone with corrugated surfaces was tested in the Langley 8-Foot High-Temperature Structures Tunnel to measure the aerodynamic heating of its surfaces. The tests were made in a turbulent boundary layer at angles of attack of 0°, 5°, and 10°. Heating of the windward side was in reasonable agreement with theoretical turbulent predictions for a smooth cone, while heating on the leeward side was between laminar and turbulent predictions as a result of local transitional flow or flow separation produced by high lee-side pressures. Localized heating measurements indicated a significant increase in heating at large cross-flow angles, with the maximum heating rates occurring where the flow reattaches on the upstream side of the corrugation crest and the minimum occurring on the downstream side where the flow is separated.

17. Key Words (Suggested by Author(s))	18. Distribution Statement
Metallic thermal protection system Blunt cone Corrugated surface Aerodynamic heating	Unclassified - Unlimited Subject Category 34

19. Security Classif. (of this report)	20. Security Classif. (of this page)	21. No. of Pages	22. Price
Unclassified	Unclassified	43	A03

For sale by the National Technical Information Service, Springfield, Virginia 22161

NASA-Langley, 1981